https://doi.org/10.1093/plcell/koac330 THE PLANT CELL 2023: 35: 827–851

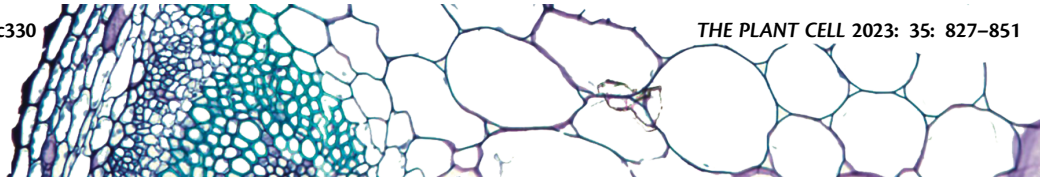

Research Article

Arabidopsis EXECUTER1 interacts with WRKY transcription factors to mediate plastid-to-nucleus singlet oxygen signaling

Yuhong Li [1,2] Hanhong Liu [1,2] Tingting Ma [1] Jialong Li [1] Jiarui Yuan [1,2] Yong-Chao Xu [3] Ran Sun [1,2] Xinyu Zhang [1,†] Yanjun Jing [1] Ya-Long Guo [2,3] and Rongcheng Lin [1,2,*]

1 Key Laboratory of Photobiology, Institute of Botany, Chinese Academy of Sciences, Beijing 100093, China
2 University of Chinese Academy of Sciences, Beijing 100049, China
3 State Key Laboratory of Systematic and Evolutionary Botany, Institute of Botany, Chinese Academy of Sciences, Beijing 100093, China

*Author for correspondence: rclin@ibcas.ac.cn (R.L.)
†Present address: Laboratoire de Reproduction et De´veloppement des Plantes, ENS de Lyon, Lyon Cedex 07, France.

Y.L. carried out the majority of the experiments; H.L. performed chromatin immunoprecipitation assays, yeast two-hybrid assays of different plant species, and bioinformatic analysis; T.M. performed EMS mutagenesis, yeast one-hybrid assays, and partial phenotypic analysis and grew the mutant library; J.L. assisted in physiological and chemical treatments; J.Y. performed part of mutant screening and gene cloning; R.S. partially participated in identifying point mutations; X.Z. participated in promoter bioinformatic analysis; Y.X. and Y.G. carried out evolutionary analysis; Y.J. participated in data analysis and comments; R.L. initiated and directed the study and wrote the paper. All authors analyzed and interpreted data and reviewed the manuscript.

The author responsible for distribution of materials integral to the findings presented in this article in accordance with the policy described in the Instructions for Authors (https://academic.oup.com/plcell/pages/General-Instructions) is: Rongcheng Lin (rclin@ibcas.ac.cn).

Abstract

Chloroplasts produce singlet oxygen ($^1O_2$), which causes changes in nuclear gene expression through plastid-to-nucleus retrograde signaling to increase plant fitness. However, the identity of this $^1O_2$-triggered pathway remains unclear. Here, we identify mutations in *GENOMES UNCOUPLED4* (*GUN4*) and *GUN5* as suppressors of *phytochrome-interacting factor1* (*pif1*) *pif3* in regulating the photo-oxidative response in *Arabidopsis thaliana*. GUN4 and GUN5 specifically interact with EXECUTER1 (EX1) and EX2 in plastids, and this interaction is alleviated by treatment with Rose Bengal (RB) or white light. Impaired expression of *GUN4*, *GUN5*, *EX1*, or *EX2* leads to insensitivity to excess light and overexpression of *EX1* triggers photo-oxidative responses. Strikingly, upon light irradiation or RB treatment, EX1 transiently accumulates in the nucleus and the nuclear fraction of EX1 shows a similar molecular weight as the plastid-located protein. Point mutagenesis analysis indicated that nuclear localization of EX1 is required for its function. EX1 acts as a transcriptional co-activator and interacts with the transcription factors WRKY18 and WRKY40 to promote the expression of $^1O_2$-responsive genes. This study suggests that EX1 may act in plastid-to-nucleus signaling and establishes a $^1O_2$-triggered retrograde signaling pathway that allows plants adapt to changing light environments during chloroplast development.

Received February 04, 2022. Accepted November 16, 2022. Advance access publication November 25, 2022

IN A NUTSHELL

Background: In response to developmental and environmental cues such as changing light intensity, plastids/chloroplasts produce, and emit signals such as singlet oxygen, $^1O_2$. These signals broadly affect the expression of nuclear genes, thereby altering chloroplast function to help the plant develop and acclimate to the changing environment. This signaling process is termed retrograde signaling. The chloroplast-localized protein EXECUTER1 (EX1) is required for $^1O_2$-triggered retrograde signaling.

Question: What are the biochemical properties of EX1 and how is $^1O_2$-mediated retrograde signaling transduced from plastids to the nucleus?

Findings: Using a forward genetic screen in *Arabidopsis thaliana*, we identified GENOMES UNCOUPLED4 (GUN4) and GUN5 as two suppressors of a *pif1 pif3* double mutant, which lacks the function of PHYTOCHROME-INTERACTING FACTOR1 (PIF1) and PIF3. GUN4 and GUN5 interacted with EX1 and its homolog EX2 in plastids, and $^1O_2$ prevented this interaction. The *gun4*, *gun5*, *ex1*, and *ex2* mutants showed increased tolerance of high light, whereas seedlings overexpressing *GUN4* or *EX1* were sensitive to photobleaching. Upon induction by $^1O_2$, EX1 transiently accumulated and translocated from plastids to the nucleus and the nuclear targeting of EX1 was required for its function. In the nucleus, EX1 interacted with the transcription factors WRKY18 and WRKY40 and functioned as a transcriptional co-activator to promote the expression of $^1O_2$-responsive genes. We propose a working model in which EX1 directly mediates retrograde $^1O_2$ signaling from plastids to the nucleus.

Next steps: We are interested in how EX1 is spatially regulated in the retrograde $^1O_2$ signaling pathway.

Introduction

Plastids (such as etioplasts and chloroplasts) are plant and algal organelles with their own genetic material that originated from an ancient endosymbiotic event between a cyanobacterium and a eukaryotic cell (Hohmann-Marriott and Blankenship, 2011). Because most plastid-localized proteins are now encoded by the nuclear genome, the tight coordination of physiological and metabolic processes and the maintenance of cellular homeostasis in the organelle require inter-organellar communication between the nucleus and chloroplasts. In response to changing developmental and environmental cues, chloroplasts produce and emit signals that broadly affect the expression of nuclear genes, thereby altering chloroplast homeostasis to improve plant growth and acclimation, a process termed retrograde signaling (reviewed in Nott et al., 2006; Chan et al., 2016; de Souza et al., 2017).

The chloroplast-to-nucleus retrograde signaling system is a complex network that can be classified into two categories: biogenic and operational controls. Biogenic signaling refers to signals generated from developing chloroplasts, whereas operational signaling reflects those sent from mature chloroplasts in response to environmental perturbations (reviewed in Pogson et al., 2008; Chan et al., 2016; Woodson, 2019). Chloroplasts rely on at least four major signals/pathways: signals related to the tetrapyrrole biosynthesis pathway; signals triggered by plastid gene expression; signals related to reactive oxygen species (ROS) and changes in photosynthetic electron transport activity; and signals derived from disturbed plastid metabolism (reviewed in Chi et al., 2013; de Souza et al., 2017; Hernandez-Verdeja and Strand, 2018).

Photosynthesis-associated nucleus-encoded genes (PhANGs) are repressed when chloroplast biogenesis is blocked. The Arabidopsis (*Arabidopsis thaliana*) *genomes uncoupled* (*gun*) mutants display a partial derepression of some PhANGs following improper chloroplast development, such as during exposure to norflurazon (Susek et al., 1993). GUN1 is a plastid-localized protein containing a pentatricopeptide repeat domain (Koussevizky et al., 2007), while GUN2–GUN6 are enzymes or regulators associated with tetrapyrrole biosynthesis (Mochizuki et al., 2001; Larkin et al., 2003; Strand et al., 2003; Pfannschmidt, 2010; Woodson et al., 2011). GUN1 is involved in regulating plastid protein homeostasis and participates in multiple retrograde signaling pathways (Hernandez-Verdeja and Strand, 2018; Wu et al., 2019; Hernandez-Verdeja et al., 2020; Wu and Bock, 2021). *GUN4* and *GUN5* encode the regulatory and the CHLH subunit of Mg-chelatase in tetrapyrrole/chlorophyll biosynthesis, respectively (Mochizuki et al., 2001; Larkin et al., 2003). GUN4 is a porphyrin-binding protein that stimulates GUN5/CHLH activity (Larkin et al., 2003; Tanaka et al., 2011). However, the signaling mechanisms mediated by GUN4 and GUN5 remain largely unclear (Terry and Smith, 2013).

Excess amounts of tetrapyrrole metabolic intermediates such as protochlorophyllide (Pchlide), which accumulates in the dark, trigger singlet oxygen ($^1O_2$) production in chloroplasts upon light exposure (op den Camp et al., 2003; Wagner et al., 2004). $^1O_2$ is also generated from chlorophyll triplet excited states in photosystem II under high light irradiance (Triantaphylides and Havaux, 2009). $^1O_2$ not only acts as a toxic oxygen molecule that oxidizes macromolecules and causes cellular damage but also initiates a retrograde signaling cascade to the nucleus that controls acclimation, stress responses, and cell death (Triantaphylidès et al., 2008; Woodson, 2019). Because of its short half-life, $^1O_2$ itself is unlikely to be the mobile signal that moves across the chloroplast envelope; it may instead

interact with other components close to its production site to generate more stable signaling molecules (Kim and Apel, 2013). Several conditional $^1O_2$-producing mutants were identified in genetic studies. For examples, the Arabidopsis *fluorescent* (*flu*) mutant accumulates photosensitizing Pchlide in the dark and rapidly generates $^1O_2$ when transferred into a light environment (Meskauskiene et al., 2001). A chlorophyll *b*-deficient mutant, *chlorina 1*, is particularly sensitive to high-light intensity and accumulates $^1O_2$, which leads to the up-regulation of hundreds of nuclear genes, followed by cell death (Ramel et al., 2013).

Two homologous thylakoid-localized proteins, EXECUTER1 (EX1) and EX2, act genetically downstream of FLU to regulate $^1O_2$-dependent stress responses (Wagner et al., 2004; Lee et al., 2007; Kim et al., 2009). EX1 undergoes a $^1O_2$-dependent post-translational oxidative modification and is subsequently degraded by the chloroplast-localized metalloprotease Filamentation temperature-sensitive H2 (FtsH2) within the grana margins of chloroplasts. FtsH2-mediated EX1 degradation is important for propagating the $^1O_2$ signal (Wang et al., 2016; Dogra et al., 2019). Accordingly, EX1 has been proposed to transmit the plastid $^1O_2$ signal and regulate nuclear gene expression (Tarahi Tabrizi et al., 2016; Dogra et al., 2018). Interestingly, EX2 also undergoes oxidative modification and FtsH-dependent turnover, which represses EX1 oxidation and degradation, thus attenuating $^1O_2$ signaling (Dogra et al., 2022). However, the biochemical properties of EX proteins and their downstream signaling pathway remain largely unknown.

We previously revealed that dark-grown (etiolated) Arabidopsis seedlings harboring loss-of-function mutations in both *PHYTOCHROME-INTERACTING FACTOR1* (*PIF1*) and *PIF3* are sensitive to high-light irradiance and accumulate $^1O_2$ in their cotyledons (Chen et al., 2013). Here, in a forward genetic screen, we unexpectedly identified *gun4* and *gun5* mutants as suppressors of the greening block (and thus chloroplast development) characteristic of the *pif1 pif3* double mutant. We showed that GUN4 and GUN5 interact with EX1 and EX2 and that $^1O_2$ stress alleviates their interaction. After illumination, EX1 rapidly accumulated in the nucleus, where it may function as a transcriptional co-activator that facilitates WRKY transcription factors in their regulation of singlet oxygen-responsive genes (*SORG*) expression. Our study reveals that EX1 is likely a mobile protein that directly delivers plastid $^1O_2$ signals to the nucleus to establish a $^1O_2$-triggered retrograde signaling cascade in plants.

Results

Mutations in *GUN4* or *GUN5* suppress *pif1 pif3* photobleaching responses

The *flu* mutant was identified as a conditional mutant that generates $^1O_2$ specifically in chloroplasts upon a dark-to-light shift and survives only under continuous light conditions (Meskauskiene et al., 2001). PIF1 and PIF3 are two key components of the light signaling pathway and their double loss-of-function mutants (*pif1 pif3*) grow normally under light–dark cycles (Ni et al., 1998; Huq et al., 2004; Chen et al., 2013). The dark-grown seedlings of both *flu* and *pif1 pif3* accumulated Pchlide intermediates, although *flu* accumulated higher Pchlide levels than *pif1 pif3* (Meskauskiene et al., 2001; Chen et al., 2013; Supplemental Figure S1A). *flu* etiolated seedlings failed to turn green (the percentage greening reflects the extent of photobleaching caused by chloroplast damage), whereas *pif1 pif3* seedlings were sensitive to increasing light intensity and severely bleached when exposed to relatively high light (~200 $\mu mol \cdot m^{-2} \cdot s^{-1}$; Supplemental Figure S1, B–D). *pif1 pif3* accumulated high levels of $^1O_2$ (as evidenced by its indirect detection with the fluorescent probe singlet oxygen sensor green, SOSG; Supplemental Figure S1E; Flors et al., 2006; Chen et al., 2013). Exogenous application of the $^1O_2$ scavenger vitamin B6 (Triantaphylides and Havaux, 2009) largely blocked $^1O_2$ accumulation in the *pif1 pif3* mutant seedlings (Supplemental Figure S1E). Furthermore, etiolated seedlings from the wild-type (WT) Columbia-0 (Col-0) accession also produced more $^1O_2$ when exposed to high light (~300 $\mu mol \cdot m^{-2} \cdot s^{-1}$) than to mild light (~80 $\mu mol \cdot m^{-2} \cdot s^{-1}$; Supplemental Figure S1F). Thus, like the *flu* mutant, *pif1 pif3* is a new genetic mutant that has advantages for the study of the $^1O_2$ response.

To explore the genetic basis of PIF1/PIF3-mediated $^1O_2$ production, we mutagenized ~25,000 *pif1 pif3* seeds with ethyl methanesulfonate (EMS) and performed a suppressor screen for *suppressor of pif1 pif3 in singlet oxygen* (*spo*) mutants. From approximately 10,000 M_2 lines, we identified over 100 independent lines with increased percentage greening compared to the *pif1 pif3* mutant. We then backcrossed these candidate suppressor lines to *pif1 pif3* and used the resulting segregating F_2 populations for mapping-by-sequencing. Analysis of the sequencing data revealed that many candidate suppressors carry point mutations in genes encoding GUN5/CHLH (=SPO1, 18 mutations) or its cofactor GUN4 (=SPO2, six mutations), leading to amino acid changes in GUN4 or GUN5 protein (Figure 1A). These residues are conserved in GUN4 or GUN5 across Arabidopsis, rice (*Oryza sativa*), and poplar (*Populus trichocarpa*; Supplemental Figure S2). The various *spo1* and *spo2* alleles (the two representative alleles *spo1-14* and *spo2-6* in the *pif1 pif3* background are shown in Figure 1) rescued the photobleaching phenotype, ROS-responsive gene expression patterns, and cell death observed in *pif1 pif3* seedlings (Figure 1, B–E; Supplemental Figure S3).

Loss-of-function mutants of *GUN4* or *GUN5* are seedling lethal (Huang and Li, 2009; Peter and Grimm, 2009). To further validate the identity of these suppressors, we obtained T-DNA insertion mutants for *gun4* (SALK_011461) and *gun5* (SAIL_138_B09), which we confirmed as knockdown alleles (Supplemental Figure S4, A and B). Either *gun4* or *gun5* mutation rescued the photobleaching response of *pif1 pif3* (Supplemental Figure S4, C–F). Consistently, a previous study

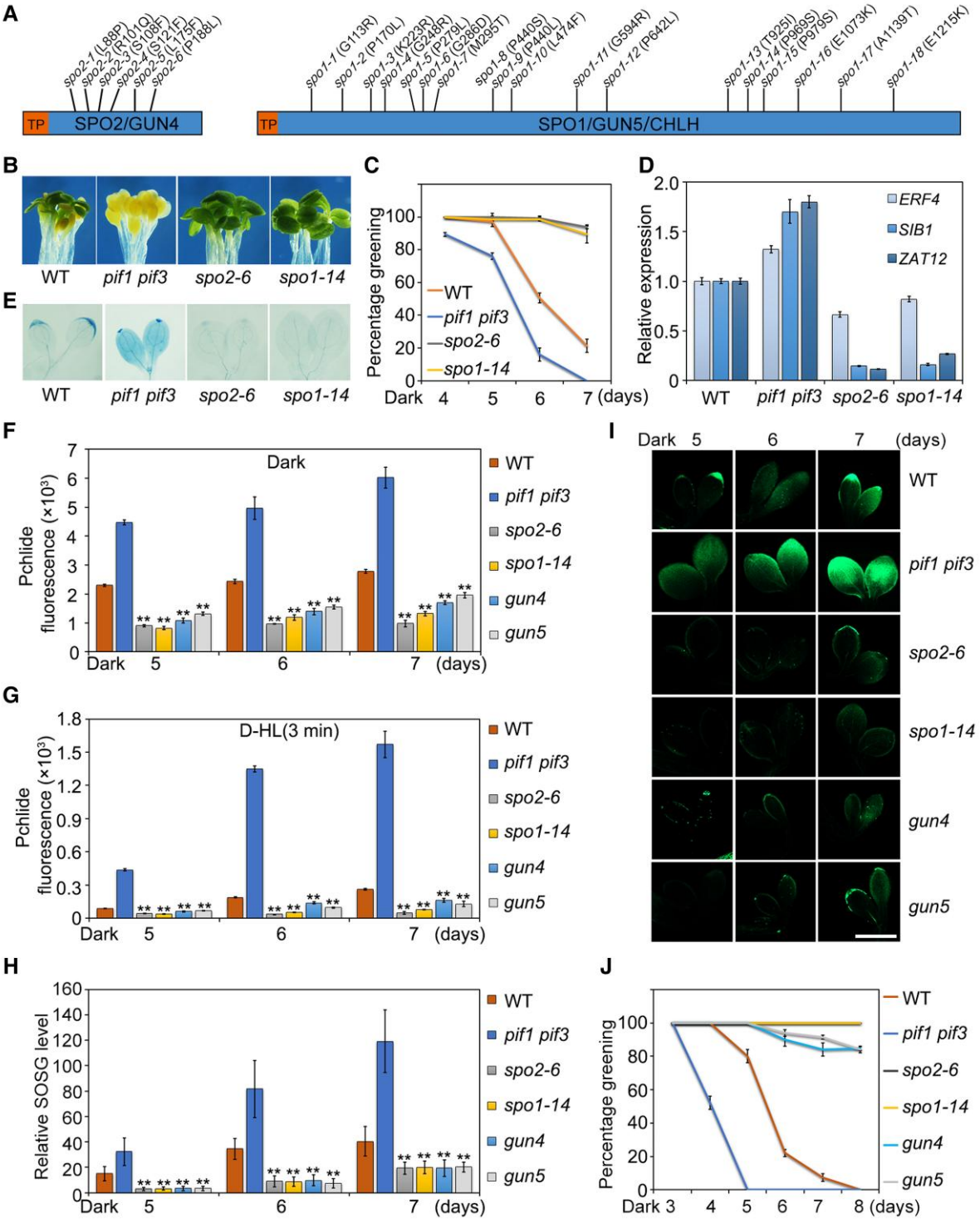

Figure 1 Mutations in *SPO2/GUN4* and *SPO1/GUN5* suppress the photobleaching phenotype of *pif1 pif3* seedlings. A, Schematic diagrams of the SPO2 (=GUN4) and SPO1 (=GUN5/CHLH) proteins and the location of the mutations identified in our collection of suppressors. TP, transit peptide. B, Cotyledon greening phenotype of *pif1 pif3* suppressors. One representative allele each for *spo2* and *spo1* mutants in the *pif1 pif3* background is shown. The 6.5-day-old etiolated seedlings were exposed to light (~80 μmol·m^{-2}·s^{-1}) for 2 days. C, Percentage greening of seedlings grown in the dark for the indicated number of days followed by illumination for 2 days. D, Relative transcript levels of three ROS-responsive genes, *ETHYLENE-RESPONSIVE TRANSCRIPTION FACTOR 4* (*ERF4*), *SIGMA FACTOR-BINDING PROTEIN 1* (*SIB1*), and *ZAT ZINC FINGER PROTEIN 12* (*ZAT12*; Chen et al., 2013). Seedlings were grown in the dark for 6.5 days, followed by 1 h of light exposure (~80 μmol·m^{-2}·s^{-1}). E, Trypan

(continued)

showed that *gun5* suppresses the greening phenotype of the *pif3* single mutant (Shin et al., 2009). Together, these data indicate that *spo2/gun4* and *spo1/gun5* are indeed suppressors of *pif1 pif3* in regulating seedling greening. We also crossed the knockdown T-DNA alleles of *GUN4* and *GUN5* into the *flu* mutant background. Mutation of *GUN4* or *GUN5* resulted in complete or partial suppression of the photobleaching phenotype of *flu*, respectively (Supplemental Figure S5), suggesting that GUN4 and GUN5 also genetically interact with FLU.

The genetic analyses suggested that the levels of GUN4/SPO2 and GUN5/SPO1 are possibly higher in the *pif1 pif3* mutant background. Consistent with this interpretation, the transcript levels of *GUN4* and *GUN5*, but not *CHLI1* or *CHLI2* (encoding the CHLI subunits of Mg-chelatase), rose remarkedly in etiolated *pif1 pif3* seedlings relative to the WT (Supplemental Figure S6A). Accordingly, the steady-state protein levels of GUN4 and GUN5 increased in *pif1 pif3* compared to WT (Supplemental Figure S6B). Previous studies showed that *GUN5* is up-regulated in the *pifq* mutant (harboring mutations in *PIF1*, *PIF3*, *PIF4*, and *PIF5*, Shin et al., 2009) and PIF3 can associate with the *GUN5* promoter in a chromatin immunoprecipitation (ChIP) assay (Liu et al., 2013). These results suggest a direct regulation of *GUN5* by PIF3. Surprisingly, the transcript levels of mutated *GUN4* and *GUN5* increased in some *spo2* and *spo1* alleles, respectively (Supplemental Figure S6C), possibly due to a negative feedback regulation of both genes. These results indicate that PIF1 and PIF3 negatively regulate *GUN4* and *GUN5* levels in the dark.

Knockdown of *GUN4* or *GUN5* leads to reduced levels of Pchlide and $^1O_2$

As GUN4 and GUN5 are the regulator and a subunit of Mg-chelatase, respectively (Larkin et al., 2003; Adhikari et al., 2011), we measured the level of the Mg-chelatase product, Mg-protoporphyrin IX (MgP), by high-performance liquid chromatography (HPLC). The *pif1 pif3* seedlings had an increased amount of MgP compared to the WT (Supplemental Figure S7A). Furthermore, MgP levels were moderately reduced in the *spo1-14* and *spo2-4* alleles and drastically decreased in the *spo1-16*, *pif1 pif3 gun5*, and *pif1 pif3 gun4* mutants, relative to *pif1 pif3* (Supplemental Figure S7A). These results indicate that PIF1/PIF3 negatively regulates MgP synthesis and that knockdown of *GUN4* or *GUN5* suppresses the response of *pif1 pif3* in mediating tetrapyrrole metabolism.

An accumulation of either free chlorophyll or its precursors (e.g. Pchlide and Proto-IX) may generate $^1O_2$ upon light irradiation (Apel and Hirt, 2004; Krieger-Liszkay et al., 2008; Triantaphylidès and Havaux, 2009). Compared to WT, both the *gun4* and *gun5* mutants had lower levels of total Pchlide in seedlings grown in the dark for different lengths (Figure 1F; Supplemental Figure S7, B and C). While WT accumulated a certain amount of free Pchlide after 3 min of high light (~300 μmol·m^{-2}·s^{-1}) treatment, Pchlide in *gun4* and *gun5* was mostly converted into chlorophyllide (Figure 1G; Supplemental Figure S7D). Accordingly, *gun4* and *gun5* accumulated less $^1O_2$ than WT upon exposure to high light (Figure 1, H and I). Partial loss of *GUN4* or *GUN5* function leads to reduced chlorophyll accumulation and growth retardation under normal conditions (Mochizuki et al., 2001; Peter and Grimm, 2009). Strikingly, after transfer to high light conditions, the percentage greening of WT gradually decreased along with a longer dark incubation period, whereas those of *gun4* and *gun5* remained high (Figure 1J). In addition, *gun4* and *gun5* had a higher percentage greening than WT when 6-day-old etiolated seedlings were exposed to 50 or 300 μmol·m^{-2}·s^{-1} light intensities (Supplemental S7, E and F). The *spo2* and *spo1* mutants responded similarly as *gun4* and *gun5* and suppressed the phenotypes of *pif1 pif3* under these conditions (Figure 1, F–J; Supplemental Figure S7). We also generated Arabidopsis transgenic lines overexpressing *GUN4* (*35S:GUN4-GFP*, cloned in-frame with the green fluorescence protein [*GFP*] sequence and driven by the cauliflower mosaic virus [CaMV] 35S promoter). Overexpression of *GUN4* resulted in severe photobleaching and significant $^1O_2$ accumulation (Supplemental Figure S8). These results indicate that GUN4 and GUN5 promote $^1O_2$ accumulation, likely largely through regulating tetrapyrrole metabolism, especially the Pchlide level.

GUN4 and GUN5 interact with EX1 and EX2

The fact that *GUN4* and *GUN5* mutations suppress the photobleaching phenotype of *pif1 pif3* and *flu*, and as EX1 and EX2 are involved in mediating $^1O_2$ signaling in chloroplasts and their loss of function partially suppresses *flu* (Wagner et al., 2004; Lee et al., 2007; Zhang et al., 2014), we set out to test the relationship between PIF1/PIF3 and EX1/EX2. We thus generated *pif1 pif3 ex1* and *pif1 pif3 ex2* triple mutants, as well as the *pif1 pif3 ex1 ex2* quadruple mutant. Phenotypic analysis showed that the *ex1* or *ex2* mutation partially suppresses photobleaching in *pif1 pif3*, while their

Figure 1 (Continued)
blue staining revealing cell death in 5-day-old etiolated seedlings exposed to light (~80 μmol·m^{-2}·s^{-1}) for 6 h. Scale bar, 0.5 mm. F, Relative Pchlide levels (emission at 636 nm) in seedlings grown in the dark for 5–7 days. G, Relative free Pchlide levels in seedlings treated with 3 min of high light (~300 μmol·m^{-2}·s^{-1}). H, Relative SOSG levels in etiolated seedlings exposed to high light (~300 μmol·m^{-2}·s^{-1}) for 1 h. More than 100 sampling dots (diameter = 100 μm, 10~15 dots in each cotyledon) were collected from at least 10 seedings for each genotype. I, Representative SOSG fluorescence of seedlings shown in (H). Scale bar, 0.5 mm. J, Percentage greening. Seedlings were grown in the dark for different lengths followed by 2 days of high light (~300 μmol·m^{-2}·s^{-1}) exposure. For, C, D, F–H, and J, data are means ± s.d., $n = 3$ ($n > 100$ for H). Asterisks indicate significant differences compared to WT using Student's t test ($P < 0.01$).

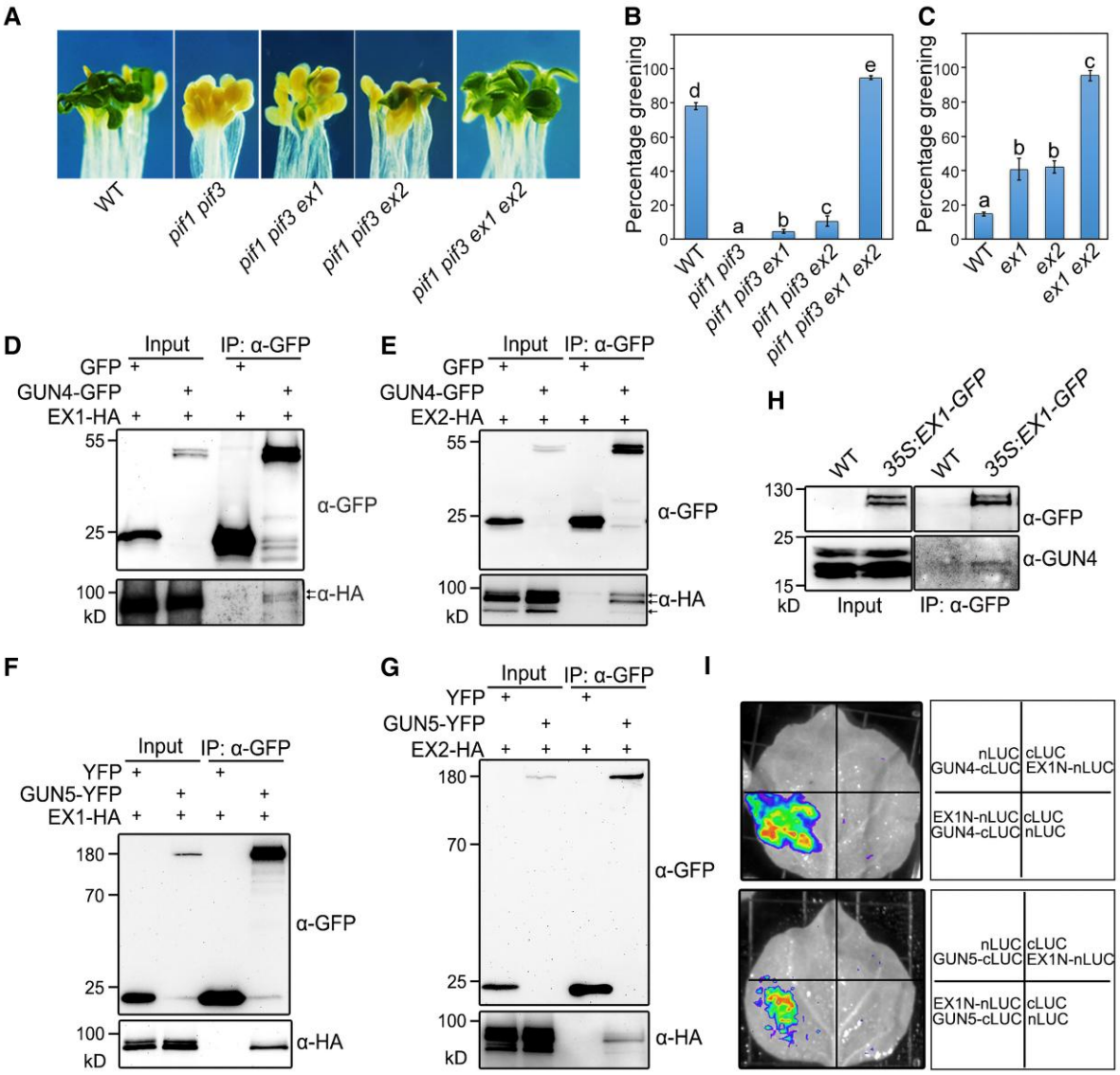

Figure 2 GUN4 and GUN5 physically interact with EX1 and EX2. A, Genetic interaction between *pif1 pif3*, *ex1-2*, and *ex2*. Seedlings were grown in the dark for 6.5 days, followed by light exposure (~80 μmol·m^{-2}·s^{-1}) for 2 days. B, Percentage greening of seedlings shown in (A). C, Percentage greening of seedlings grown in the dark for 5.5 days, followed by 2-day exposure to high light (~300 μmol·m^{-2}·s^{-1}). For B and C, data are means ± s.d., $n = 3$. Different lowercase letters indicate significant differences by two-way ANOVA ($P < 0.01$). D and E, Co-IP assays between GUN4-GFP and EX1-HA (D) or EX2-HA (E) in Arabidopsis protoplasts. F and G, Co-IP assays between GUN5-YFP and EX1-HA (F) or EX2-HA (G) in protoplasts. Expression of *GFP* or *YFP* served as controls. Transfected protoplasts expressing various constructs were incubated in the dark for 16 h. H, Co-IP assay in WT and *35S:EX1-GFP*. I, LCI assay. The indicated constructs were co-infiltrated into *N. benthamiana* leaves, followed by 2 days of growth under long-day conditions before LUC imaging.

combination completely blocked photobleaching (Figure S2, A and B), suggesting that EX1 and EX2 additively and genetically interact with PIF1 and PIF3. The *ex1* and *ex2* single mutants and especially the *ex1 ex2* (*ex1-3 ex2-2*) double mutant seedlings had lower Pchlide levels than the WT in the dark (Supplemental Figure S9A), suggesting that EX1 and EX2 are involved in regulating Pchlide biosynthesis. The high accumulation of Pchilde in *pif1 pif3* was completely lost in the *pif1 pif3 ex1 ex2* quadruple mutant (Supplemental Figure S9B). Notably, the *ex1* and *ex2* mutants were more resistant to high light than the WT, as shown by their percentage greening; greening was further enhanced in *ex1 ex2* (Figure 2C).

Given the similar responses to high-light stress exhibited by their respective mutants and their localization to the chloroplast, we hypothesized that GUN4/GUN5 and EX1/EX2 might physically interact. To test this hypothesis, we first performed transient expression and co-immunoprecipitation (co-IP) experiments in Arabidopsis protoplasts. GUN4-GFP co-immunoprecipitated full-length EX1-HA (tagged with 3×

hemagglutinin [HA]) and EX2-HA when using an anti-GFP antibody for immunoprecipitation upon co-transfection of protoplasts maintained in the dark (Figure 2, D and E). Similarly, GUN5-YFP (yellow fluorescence protein) also pulled down EX1-HA and EX2-HA in co-transfected protoplasts (Figure 2, F and G). An in vivo co-IP assay showed that anti-GFP antibody immunoprecipitates GUN4 in a stable *35S:EX1-GFP* transgenic line (see below for detailed information), but not in the WT control (Figure 2H). These results indeed reveal that GUN4/GUN5 interacts with EX1/EX2.

Next, we visualized their interaction by infiltrating *Nicotiana benthamiana* leaves. For an unknown reason, the expression level of full-length *EX1* in *N. benthamiana* was very low. We thus divided EX1 and EX2 into their N-terminal fragments (278 amino acids [aa] containing the chloroplast transit peptide and the UvrB/C motif [pfam02151]; designated EX1N and EX2N) and C-terminal portions containing the DUF3506 domain (406 aa for EX1; 373 aa for EX2; designated EX1C and EX2C; Supplemental Figure S10A). A luciferase (LUC) complementation imaging (LCI) assay showed that GUN4-cLUC (GUN4 fused to the C-terminal fragment of LUC) and GUN5-cLUC interact with EX1N-nLUC (EX1N fused to the N-terminal part of LUC) to reconstitute luciferase activity in *N. benthamiana* leaves (Figure 2I). A bimolecular fluorescence complementation (BiFC) assay showed that co-infiltration of *EX1N-nYFP* (encoding EX1N fused to an N-terminal fragment of YFP) and *GUN4-cYFP* (encoding GUN4 fused to a C-terminal fragment of YFP) reconstituted functional YFP, as evidenced by yellow fluorescence in the chloroplasts of *N. benthamiana* leaves (Supplemental Figure S10B). Furthermore, both EX1N and EX2N (fused to the yeast GAL4 activation domain), but not EX1C or EX2C, interacted with GUN4 (fused to the GAL4 DNA-binding domain) in a yeast two-hybrid assay (Supplemental Figure S10C). However, full-length EX1 and EX2 failed to interact with GUN4, possibly due to the masking effect of the EX1 C terminus in yeast cells. These results confirm that EX1 and EX2 directly interact with GUN4 and GUN5 via their N termini.

The GUN4/GUN5-EX1 interaction is alleviated by RB and light treatments

We then asked whether the $^1O_2$ signal regulated the interaction between GUN4/GUN5 and EX1. Rose Bengal (RB) functions as a photosensitizer by transferring energy to O_2, yielding $^1O_2$ (Lamberts and Neckers, 1985). To confirm the specificity of RB action in chloroplasts, we grew 5-day-old WT seedlings in the dark and exposed them to light (~80 $\mu mol \cdot m^{-2} \cdot s^{-1}$) for 30 min in the absence or presence of 100 μM RB. We quantified $^1O_2$ levels in different tissues and cellular fractions by measuring SOSG fluorescence (Flors et al., 2006). We observed that the amounts of SOSG fluorescence in cotyledons (generally harboring developed chloroplasts) are remarkedly higher after light treatment and further increase in the presence of RB, compared to darkness. However, fluorescence signals in the hypocotyls (mostly with plastids) were very low regardless of light and RB treatments (Supplemental Figure S11, A and B). In particular, SOSG fluorescence levels in chloroplasts increased upon light and RB treatments, whereas cytoplasmic SOSG levels remained very low within cotyledon cells (Supplemental Figure S11, C and D). Consistently, RB treatment significantly activated the expression of $^1O_2$ marker genes (Supplemental Figure S11E). These results suggest that RB treatment triggers $^1O_2$ production largely in chloroplasts. We therefore used this treatment in the following experiments.

First, we applied RB to Arabidopsis protoplasts in the light after transfection and 16 h of dark incubation and performed a co-IP experiment. In the absence of RB, GUN4-GFP or GUN5-YFP pulled down EX1-HA in protoplasts, as shown in Figure 2; however, a 10- to 15-min treatment with 50 μM RB strongly decreased the amount of immunoprecipitated EX1-HA (Figure 3, A and B). Second, we irradiated dark-incubated protoplasts with 40 $\mu mol \cdot m^{-2} \cdot s^{-1}$ white light and determined that less EX1-HA is co-precipitated by GUN4-GFP or GUN5-YFP after light illumination for 10–30 min relative to those kept in the dark (Figure 3, C and D). Furthermore, we conducted the co-IP assays using an *ex1 proEX1:gEX1-GFP* complementation line, in which the genomic *EX1* region was cloned in-frame with *GFP* and was driven by the *EX1* promoter (Wang et al., 2016). We attempted the experiment using dark-grown seedlings, followed by light treatment of various durations; however, GUN4 did not accumulate much in the dark, precluding any conclusive analysis. We thus grew seedlings under different light intensities. Notably, the amounts of GUN4 co-immunoprecipitated by EX1-GFP gradually decreased under increasing light intensities (from 5 to 50 $\mu mol \cdot m^{-2} \cdot s^{-1}$), possibly due to increased production of $^1O_2$ (Figure 3E). Thus, we propose that GUN4/GUN5 interact with EX1 in the absence of $^1O_2$ stress and that the $^1O_2$ signal alleviates this interaction.

EX1 localizes to the nucleus upon RB and light treatments

To further investigate the signal transduction mechanism mediated by EX1, we generated multiple *EX1* overexpression transgenic lines: *35S:EX1-GFP* (encoding full-length EX1 fused to GFP), *35S:TP-GFP-EX1* (encoding the EX1 transit peptide fused to GFP at the N terminus of EX1), and *35S:EX1-FLAG* (encoding EX1 fused to a FLAG tag; Supplemental Figure S12A). Pchlide levels increased moderately upon overexpression of *EX1* (Supplemental Figure S9C). We determined that all etiolated transgenic seedlings exhibit a lower percentage greening after light exposure (~80 $\mu mol \cdot m^{-2} \cdot s^{-1}$) when compared to the WT (Figure 4A), suggesting that overexpressing *EX1* confers a photo-oxidative response and inhibits seedling greening. Importantly, constitutive expression

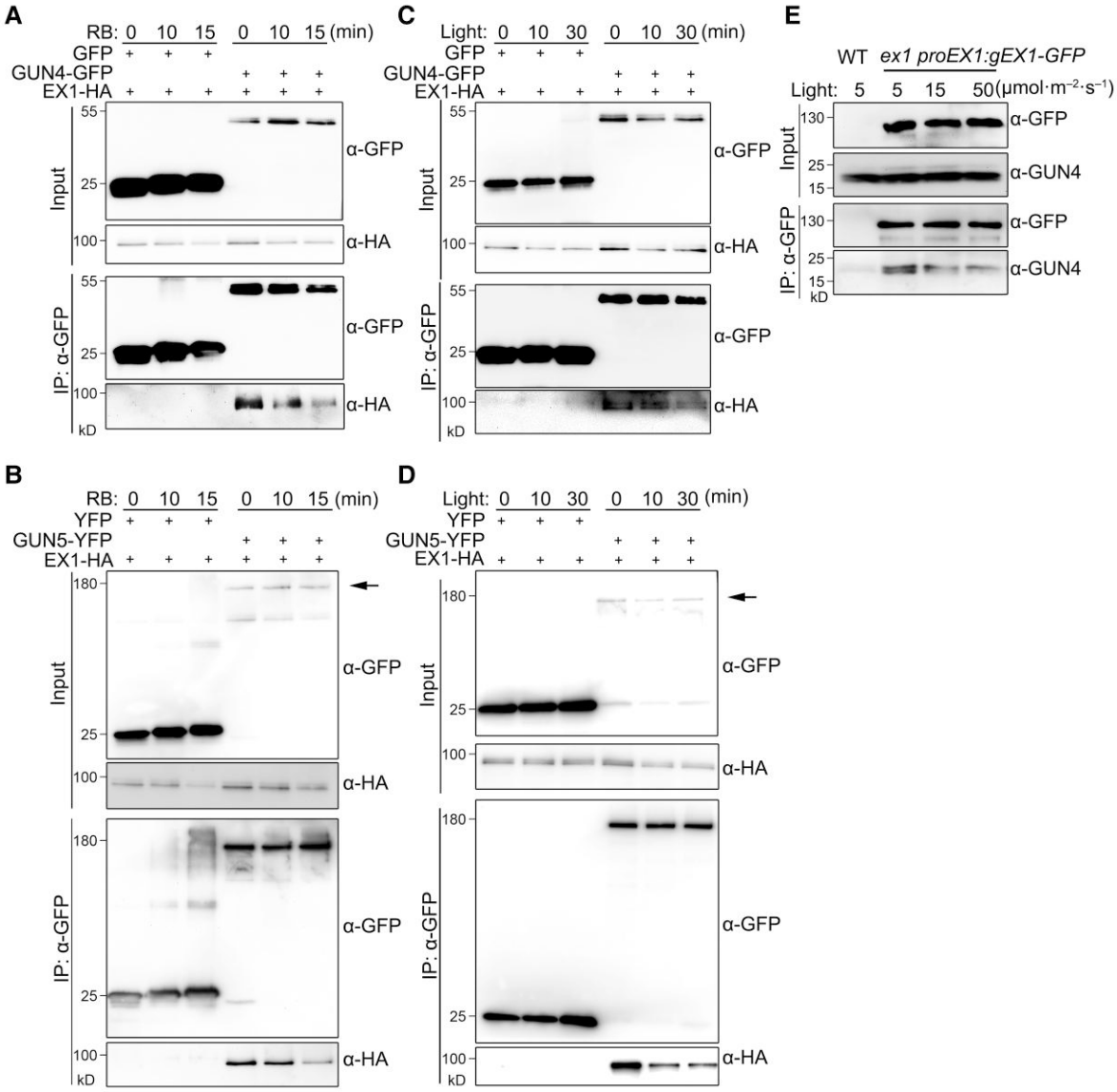

Figure 3 The GUN4/GUN5-EX1 interaction is repressed by RB and light treatments. A and B, Co-IP assays between EX1-HA and GUN4-GFP (A) or GUN5-YFP (B) in protoplasts upon RB treatment. Transfected protoplasts were incubated in the dark for 16 h and treated with 50 μM RB for the indicated time. C and D, Co-IP assays between EX1-HA and GUN4-GFP (C) or GUN5-YFP (D) in protoplasts upon light treatment. Transfected protoplasts were incubated in the dark for 16 h and illuminated (~40 μmol·m^{-2}·s^{-1}) for up to 30 min. Arrows indicate the GUN5-YFP bands. E, Co-IP assay of Col-0 (WT) and *ex1 proEX1:gEX1-GFP* seedlings grown under different light intensities and long-day conditions for 7 days.

of *EX1* (*35S:EX1-FLAG* and *35S:TP-GFP-EX1*) rescued the *ex1* mutant phenotypes (Supplemental Figure S12, B and C), demonstrating that the transgenes have a similar function as endogenous *EX1*.

We then examined the subcellular localization of the GFP fusion proteins and detected GFP fluorescence in chloroplasts of *35S:EX1-GFP* in the absence of RB treatment. Notably, we detected fluorescence in both chloroplasts and nuclei after RB treatment (Figure 4B). The GFP fusion protein in *ex1 proEX1:gEX1-GFP* exhibited a similar dual localization pattern in the presence of RB, whereas we detected no nuclear GFP fluorescence in *35S:GUN4-GFP* after RB application (Figure 4B). Furthermore, we observed GFP signals only in plastids of dark-grown *ex1 proEX1:gEX1-GFP* seedlings; however, we detected GFP fluorescence in both chloroplasts and nucleus after light illumination (~200 μmol·m^{-2}·s^{-1}; Figure 4C).

EX1 undergoes oxidative post-translational modification and FtsH2 protease-mediated degradation (Wang et al., 2016; Dogra et al., 2019). We thus extracted total and nuclear proteins and examined their dynamic regulation by immunoblot assays. RB treatment resulted in a rapid rise in total EX1 protein levels, followed by a decrease in *ex1 proEX1:gEX1-GFP* and *35S:EX1-FLAG* seedlings; this pattern was unique to EX1, as other tested chloroplast-localized proteins were not affected by RB treatment (Supplemental Figure S13, A and B).

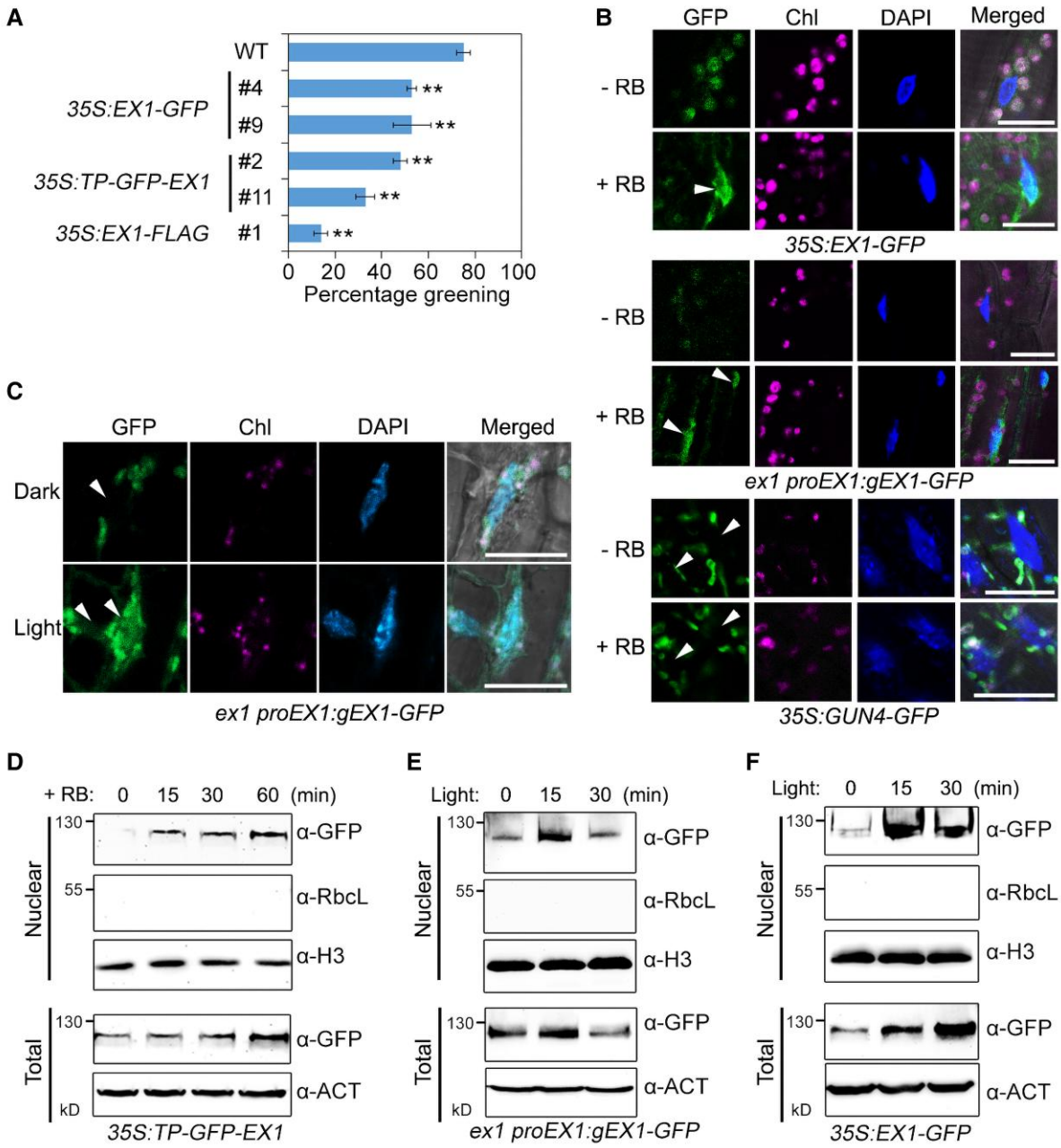

Figure 4 EX1 is present in the nucleus upon RB and light treatments. A, Percentage greening of seedlings grown in the dark for 6.5 days followed by light exposure (~80 μmol·m^{-2}·s^{-1}) for 2 days. Data are means ± s.d., $n = 3$. Asterisks indicate significant differences from WT using Student's *t* test ($P < 0.01$). B, Subcellular localization. Seedlings were grown in white light (~80 μmol·m^{-2}·s^{-1}) for 6 days and then incubated with 100 μM RB for 15 min or mock-treated (equal volume of liquid MS). The magenta channel indicates chlorophyll (Chl) autofluorescence and 4′,6-diamidino-2-phenylindole (DAPI) staining shows nuclei. Arrowheads point to nuclei. Scale bars, 20 μm. C, Subcellular localization. *ex1 proEX1:gEX1-GFP* seedlings were grown in the dark for 6.5 days followed by darkness or illumination (~200 μmol·m^{-2}·s^{-1}) for 30 min. Arrowheads point to nuclei. Scale bars, 20 μm. D, Immunoblot analysis. *35S:TP-GFP-EX1* seedlings were grown in white light (~80 μmol·m^{-2}·s^{-1}) for 6 days and treated with 100 μM RB for up to 60 min. E and F, Immunoblot analysis. *ex1 proEX1:gEX1-GFP* (E) and *35S:EX1-GFP* (F) seedlings were grown in the dark for 5.5 days, followed by illumination (~80 μmol·m^{-2}·s^{-1}) for up to 30 min. For D–F, total and nuclear fraction proteins were probed with various antibodies. Histone 3 (H3) antibody indicates nuclear proteins and RbcL antibody indicates chloroplast proteins.

Intriguingly, the GFP fusion proteins showed a rapid (15 min) and pronounced increase in abundance in the nucleus in *35S:TP-GFP-EX1* seedlings upon RB treatment (Figure 4D). EX1-GFP abundance also increased (15 min) and then decreased (30 min) in the nucleus of *ex1 proEX1:gEX1-GFP* seedlings after light irradiation (~80 μmol·m^{-2}·s^{-1}; Figure 4E). Nuclear EX1-GFP levels also increased and then slightly decreased in *35S:EX1-GFP* (Figure 4F), while the total

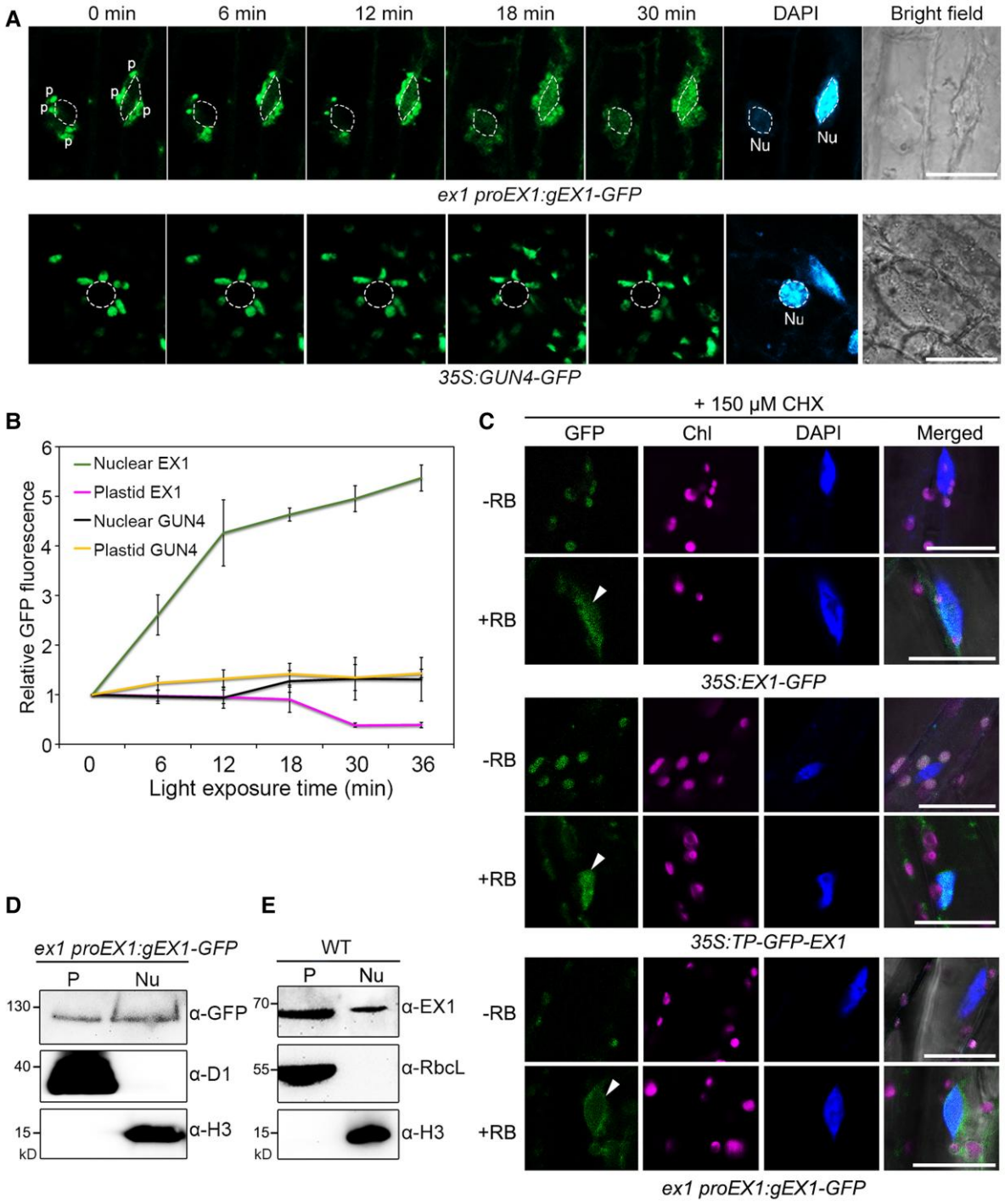

Figure 5 The nuclear fraction of EX1 likely relocates from the plastids. A, Time course of GFP fluorescence within the same cell in *ex1 proEX1:gEX1-GFP* and *35S:GUN4-GFP* seedlings during a dark-to-light transition. The seedlings were first grown in the dark for 6.5 days and then transferred to light (~200 μmol·m^{-2}·s^{-1}) for the indicated time. Dashed circles indicate nuclei (Nu) and "P" stands for plastids. Scale bars, 20 μm. B, Quantification of GFP signal levels in the nucleus and plastids in (A). Relative levels in the nuclei and plastids before light treatment were set to 1.0. Data are means ± s.d. from at least six cells. C, Subcellular localization. Seedlings were treated with 150 μM CHX for 1.5 h, followed by incubation with 100 μM RB for 15 min. Chl, chlorophyll autofluorescence. Arrowheads point to nuclei. Scale bars, 25 μm. D and E, Immunoblot analysis of proteins isolated from plastids (P) and nuclei (Nu) of *ex1 proEX1:gEX1-GFP* (D) or WT (E) seedlings grown in the dark for 6 days followed by 15 min of light exposure (~80 μmol·m^{-2}·s^{-1}). Anti-Histone H3 antibody indicates nuclear proteins and anti-RbcL or anti-D1 (a core subunit of photosystem II reaction center) antibodies indicate chloroplast proteins.

and plastid fraction levels increased with 30 min of light exposure (Supplemental Figure S13C). Different $^1O_2$ production caused by RB concentrations or light intensities may account for the different peaks of EX1 accumulation in these experiments. These data together suggest that EX1 localizes in plastids/chloroplasts in the absence of the $^1O_2$ signal and is present in the nucleus in response to $^1O_2$.

The nuclear fraction of EX1 likely relocates from the plastids

A previous mass spectrometry study showed that the mature EX1 protein in chloroplasts lacks the N-terminal 46-aa signal peptide (Dogra et al., 2019). To determine whether nucleus-localized EX1 protein was derived from plastids, we did the following experiments. First, we monitored EX1-GFP fluorescence within the same cell in the *ex1 proEX1:gEX1-GFP* seedlings to trace the dynamic translocation of EX1 during the dark-to-light transition. In the dark, we clearly detected GFP fluorescence in the plastids. However, upon light exposure, EX1-GFP signal levels gradually increased in the nucleus, while they slightly decreased in the plastids (Figure 5, A and B), providing cellular evidence that EX1 is likely transported from the plastids to the nucleus. As a negative control, we observed constitutive GUN4-GFP fluorescence in the plastids (Figure 5, A and B). Second, we investigated the subcellular localization of EX1-GFP in *35S:EX1-GFP*, *35S:TP-GFP-EX1*, and *ex1 proEX1:gEX1-GFP* seedlings treated with cycloheximide (CHX), which inhibits new protein translation. We established that CHX has no effect on the nuclear localization pattern of EX1-GFP upon RB treatment (Figures 5C and 4B), further indicating that the accumulation of EX1 in the nucleus is possibly caused by physical relocation rather than by new translation. Third, we isolated proteins from the plastid/chloroplast and nuclear fractions from *ex1 proEX1:gEX1-GFP* and performed an immunoblot assay. As shown in Figure 5D, the molecular weight of EX1-GFP in the nuclear portion was similar to that in the plastid fraction. Moreover, we generated an anti-EX1 polyclonal antibody, which recognized an approximately expected 65-kD band in the WT and a much fainter band in the *ex1* mutant (Supplemental Figure S13D). We performed an immunoblot assay in WT seedlings using anti-EX1 antibody and determined that nuclear EX1 has the same apparent molecular weight as plastid-localized EX1 (Figure 5E), further suggesting that nuclear EX1 likely does not contain the transit peptide, and thus does not come directly from the cytosol after new translation. Therefore, we propose that the $^1O_2$ signal triggers the relocation of EX1 from plastids/chloroplasts to the nucleus.

Four lysine residues are required for EX1 nuclear targeting

Next, we wished to identify the nuclear localization signal (NLS) of EX1 using cNLS Mapper (https://nls-mapper.iab.keio.ac.jp/cgibin/NLS_Mapper_form.cgi; Kosugi et al., 2009). A putative bipartite NLS sequence was predicted in aa 474–504. We thus generated GFP-fusion constructs harboring various deletions and investigated GFP localization upon their transient expression in *N. benthamiana* epidermal leaf cells (Figure 6A). Deletion of the C-terminal fragments (EX1-N506-GFP, contains the N-terminal 506 aa including the transit peptide; and EX1-N474-GFP) showed GFP fluorescence in the nucleus (Figure 6B), suggesting that the predicted NLS (aa 474–504) is not essential for EX1 nuclear targeting. We then checked the EX1 sequence in more detail and identified four lysine residues from aa 256 to 265 (Figure 6A). Expression of *EX1-N278-GFP* (encoding the N-terminal 278 aa of EX1) resulted in GFP fluorescence in the nucleus and chloroplasts, whereas expression of *EX1-N251-GFP* abrogated the nuclear GFP signals (Figure 6B), suggesting that the fragment from aa 252-278 is required for nuclear targeting. Importantly, point mutations of the lysine residues to alanine in EX1–N278 (EX1-N278^{K256A,K257A}-GFP, EX1-N278^{K263A,K265A}-GFP, or EX1-N278^{K256A,K257A,K263A,K265A}-GFP [EX1-N278^{4KA}-GFP]) also abolished the nuclear localization of the corresponding fusion proteins (Figure 6C). These data suggest that the four lysine residues in the 256–265 aa sequence of EX1 are essential for its nuclear localization. Consistently, expressing *TP-EX1-C-GFP* (containing the transit peptide and the aa 279–684 fragment) produced fluorescence only in chloroplasts (Figure 6B).

To further confirm the biological function of these lysine residues, we generated *35S:EX1*^{K256A,K257A,K263A,K265A}*-GFP* (*35S:EX1*^{4KA}*-GFP*) transgenic plants with comparable protein abundance to *35S:EX1-GFP* in the *ex1* mutant background (Supplemental Figure S12D). We observed no GFP fluorescence in the nucleus of *35S:EX1*^{4KA}*-GFP*, compared to *35S:EX1-GFP*, after RB or light treatments (Figure 6, D and E). Strikingly, *35S:EX1*^{4KA}*-GFP* failed to rescue the greening phenoty pe of the *ex1* mutant (Figure 6F). These results demonstrate that nuclear localization of EX1 is required for its function.

EX1 interacts with WRKY transcription factors

The subcellular destination of EX1 in the nucleus prompted us to investigate how it might execute its molecular function. A previous study showed that $^1O_2$ induces the expression of over 160 *SORG*s (Dogra et al., 2017). Sequence analysis revealed that *SORG* promoters are highly enriched in putative W-boxes (TTGACC/T; Supplemental Figure S14A), which are recognized by WRKY-type transcription factors (Rushton et al., 2010). We hypothesized that EX1 might associate with WRKY transcription factors to enact its molecular function in the nucleus. To test this possibility, we selected several WRKYs whose expression patterns respond to ROS and performed a yeast two-hybrid assay (Laloi et al., 2007). Indeed, we observed an interaction between EX1N or EX2N fused to the GAL4 activation domain (GAD) and WRKY15, WRKY18, WRKY40, WRKY60, and WRKY70 fused to the GAL4-binding domain (GBD) in yeast cells (Supplemental

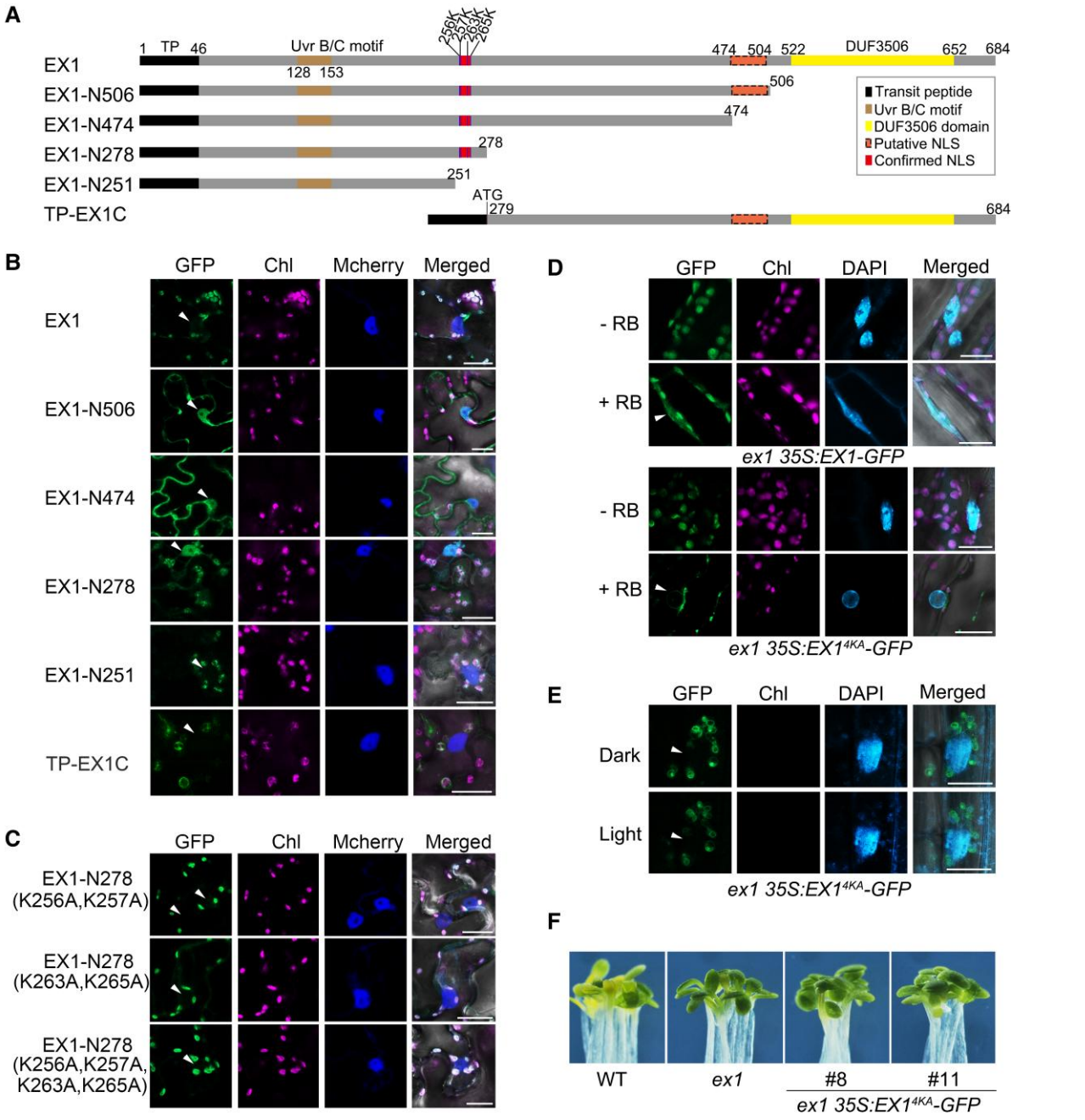

Figure 6 Identification of EX1 nuclear localization signal. A, Schematic diagrams of EX1 and its truncations. B and C, Transient protein localization assay. Various constructs encoding deletions (B) or point mutations (C) were co-infiltrated with a plasmid harboring mCherry into *N. benthamiana* epidermal leaf cells and allowed to be expressed under LD conditions for 2 days. Chl, chlorophyll autofluorescence. Arrowheads point to nuclei. Scale bars, 20 μm. D, Subcellular localization. Seedlings were grown in white light (~80 μmol·m^{-2}·s^{-1}) for 6 days and then incubated with 100 μM RB for 15 min or mock-treated (equal volume of liquid MS). Arrowheads point to nuclei. Scale bars, 20 μm. E, Subcellular localization. Seedlings were grown in the dark for 6.5 days and then transferred to light (~200 μmol·m^{-2}·s^{-1}) for 30 min. Scale bars, 20 μm. Arrowheads point to nuclei. F, Greening phenotype of seedlings grown in the dark for 6.5 days followed by light exposure (~80 μmol·m^{-2}·s^{-1}) for 2 days.

Figure S14B). We selected WRKY18 and WRKY40 due to the availability of available genetic materials to characterize their interaction with EX1 in more detail. In a transient co-IP assay, WRKY18-GFP and WRKY40-GFP immunoprecipitated more EX1-HA in Arabidopsis protoplasts after light exposure (~40 μmol·m^{-2}·s^{-1}) than in the dark (Figure 7, A and B). Similarly, WRKY18-GFP and WRKY40-GFP, but not GFP alone, pulled down an increased amount of EX1-HA, upon RB treatment (Figure 7, C and D). An LCI assay showed that co-expression of *EX1N-nLUC* and *WRKY40-cLUC*

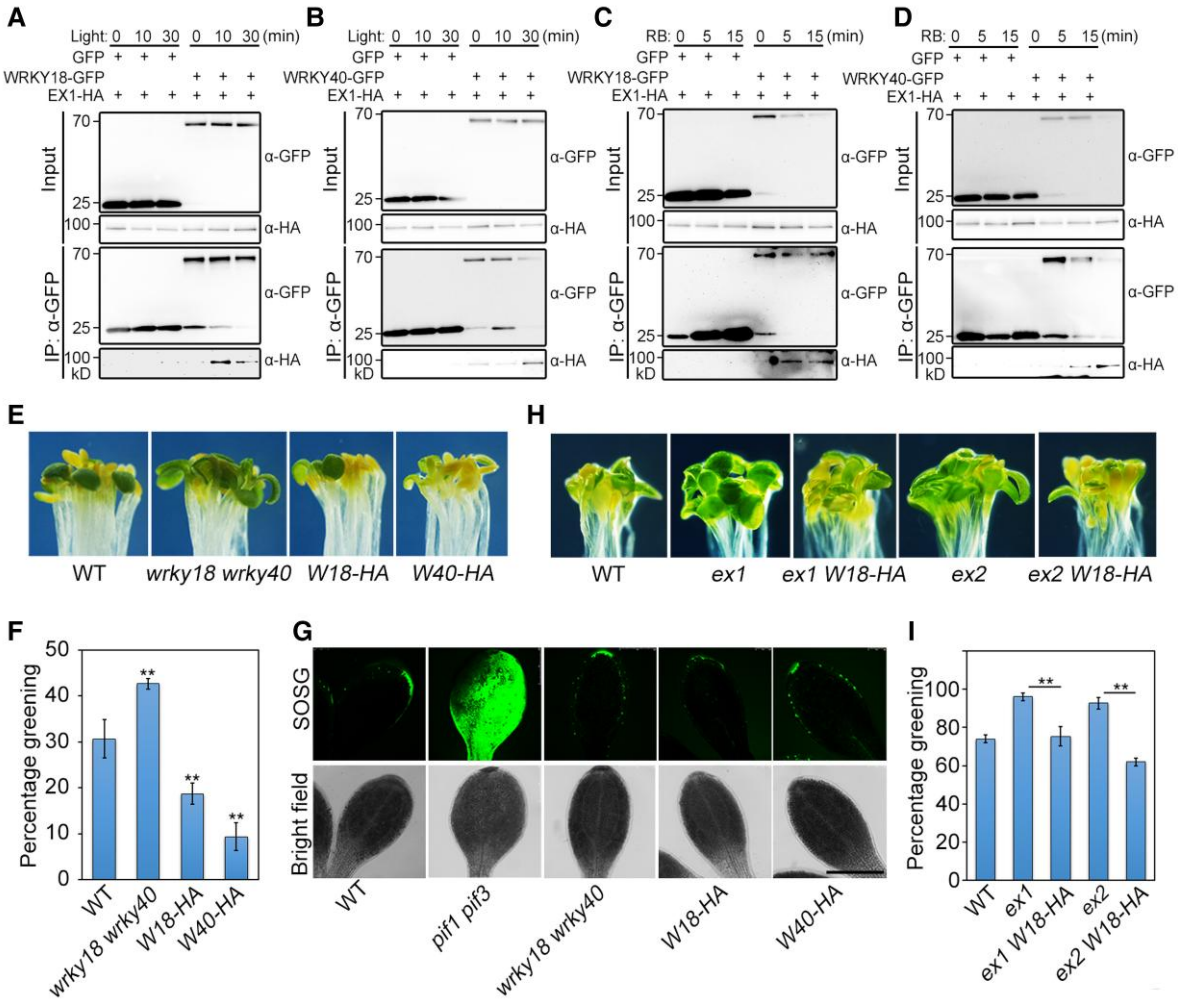

Figure 7 EX1 interacts with WRKY18 and WRKY40 and both WRKYs regulate seedling greening. A and B, Co-IP assays between EX1-HA and WRKY18-GFP (A) or WRKY40-GFP (B) in Arabidopsis protoplasts during light exposure (~40 μmol·m^{-2}·s^{-1}). C and D, Co-IP assays between EX1-HA and WRKY18-GFP (C) or WRKY40-GFP (D) in protoplasts upon 50 μM RB treatment. Expression of *GFP* serves as control. Transfected protoplasts were incubated in the dark for 16 h. E, Greening phenotype of the double mutant and transgenic lines of *WRKY18* and *WRKY40*. F, Percentage greening of seedlings shown in (E). G, SOSG fluorescence. Scale bar, 0.5 mm. H, Greening phenotype showing the genetic relationship between *ex1-2*, *ex2*, and *WRKY18-HA*. I, Percentage greening of seedlings shown in (H). For E-I, seedlings were grown in the dark for 5.5 days, followed by illumination (~300 μmol·m^{-2}·s^{-1}) for 2 days (E, F, H, and I) or 1 h (G). For F and I, data are means ± s.d., $n = 3$. Asterisks indicate significant differences using Student's *t* test ($P < 0.01$).

produces luciferase signals in *N. benthamiana* leaves (Supplemental Figure S14C). Furthermore, an in vivo co-IP assay showed that WRKY18-HA immunoprecipitates EX1 in *proWRKY18:WRKY18-HA* (*W18-HA*) transgenic seedlings after light irradiation (~80 μmol·m^{-2}·s^{-1}) but not in non-transgenic seedlings (Supplemental Figure S14D). We conclude that EX1 and WRKY18/40 physically interact and that their interaction is promoted by the $^1O_2$ signal, likely due to the increased import of EX1 into the nucleus.

Next, we sought to examine whether both WRKY factors are involved in regulating the photo-oxidation response. Transgenic seedlings expressing *W18-HA* or *proWRKY40:WRKY40-HA* (*W40-HA*) exhibited a photobleaching phenotype, whereas the *wrky18 wrky40* double mutant showed reduced sensitivity to high light (~300 μmol·m^{-2}·s^{-1}) compared to the WT, as evidenced by the significantly higher percentage greening of the double mutant (Figure 7, E and F). However, mutations or transgenes of *WRKY18* and *WRKY40* did not drastically affect Pchlide levels or $^1O_2$ accumulation (Supplemental Figure S9D; Figure 7G). Genetic analysis further showed that *W18-HA* suppresses the high percentage greening of *ex1* and *ex2* mutants (Figure 7, H and I), indicating that WRKY18 acts downstream of EX1 and EX2. These results reveal that WRKY18 and WRKY40 are indeed involved in regulating the photo-oxidation response.

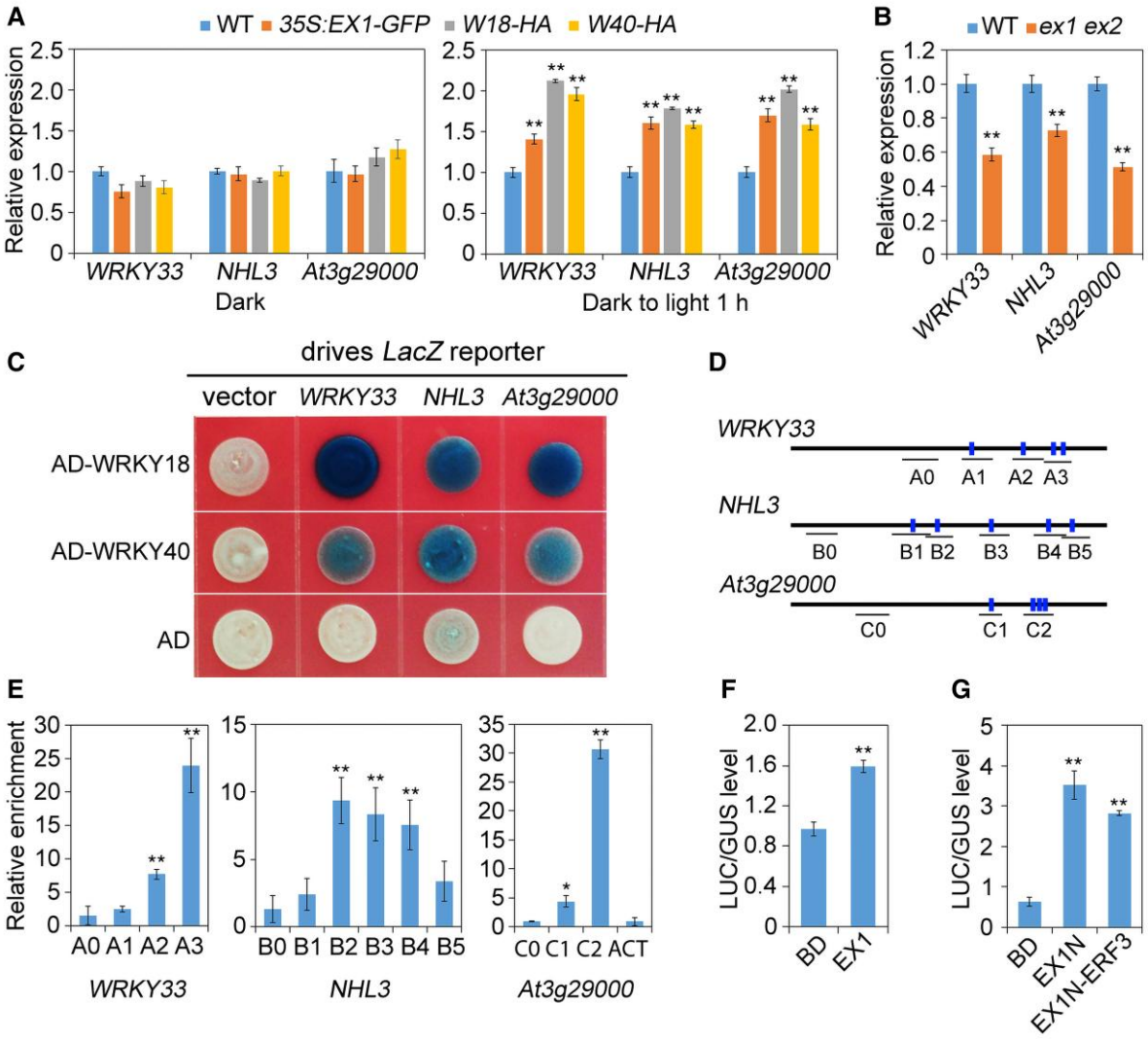

Figure 8 EX1 and WRKY18/40 coregulate SORGs expression. A and B, RT-qPCR analysis of three selected SORGs. Seedlings were grown in the dark for 5.5 days (A), followed by high light exposure (B, ~300 μmol·m^{-2}·s^{-1}) for 1 h. Asterisks indicate significant differences from Col-0 (WT) using Student's *t* test ($P < 0.01$). C, Y1H assay. AD-WRKY18, AD-WRKY40, or AD control and various LacZ reporters were co-transformed in yeast strain EGY48. D, Schematic diagram of W-boxes (bars) and PCR amplicons in the promoter regions of SORGs. E, Chromatin immunoprecipitation (ChIP) assay. *W18-HA* seedlings were grown in the dark for 6.5 days, followed by light exposure (~200 μmol·m^{-2}·s^{-1}) for 1 h. Data are means ± s.d., $n = 3$. Asterisks indicate significant differences from amplicon "X0" using Student's *t* test (**$P < 0.01$ or *$P < 0.05$). F and G, Transcriptional activation assay of full-length (F) and N-terminal EX1 (G). GAL4 DNA-binding domain (BD)-fusion constructs were co-transfected with the *GAL4pro:LUC* reporter construct into Arabidopsis protoplasts. Relative LUC activity was normalized to the activity of the GUS control (*35S:GUS*). Data are means ± s.d., $n = 3$. Asterisks indicate significant differences from BD using Student's *t* test ($P < 0.01$).

EX1 and WRKY18/40 regulate *SORGs* expression

To dissect the biochemical function of the EX1-WRKY18 interaction, we determined the regulation of three *SORGs*: *WRKY33* (At2g38470), *NDR1/HIN1-LIKE 3* (*NON-RACE-SPECIFIC DISEASE RESISTANCE1* [*NDR1*], *HAIRPIN-INDUCED* [*HIN1*]*-LIKE3* or *NHL3*, At5g06320), and At3g29000 (Dogra et al., 2017). Their transcript levels were significantly up-regulated in *35S:EX1-GFP*, *W18-HA*, and *W40-HA* transgenic seedlings upon 1 h of light treatment (~80 μmol·m^{-2}·s^{-1}), but not in the dark (Figure 8A). The expression of these three genes was down-regulated in the *ex1 ex2* double mutant after 1 h of light exposure (Figure 8B). Next, we examined whether WRKY18 directly regulated *SORGs* expression. A yeast one-hybrid assay showed that AD-WRKY18 (WRKY18 fused to the B42 activation domain) and AD-WRKY40 can bind to the promoters of *WRKY33*, *NHL3*, and At3g29000 and activate the transcription of the downstream *LacZ* reporter (Figure 8C). Furthermore, a ChIP assay using *W18-HA* seedlings and an anti-HA antibody indicated that WRKY18 associates with *SORGs* promoter regions containing the

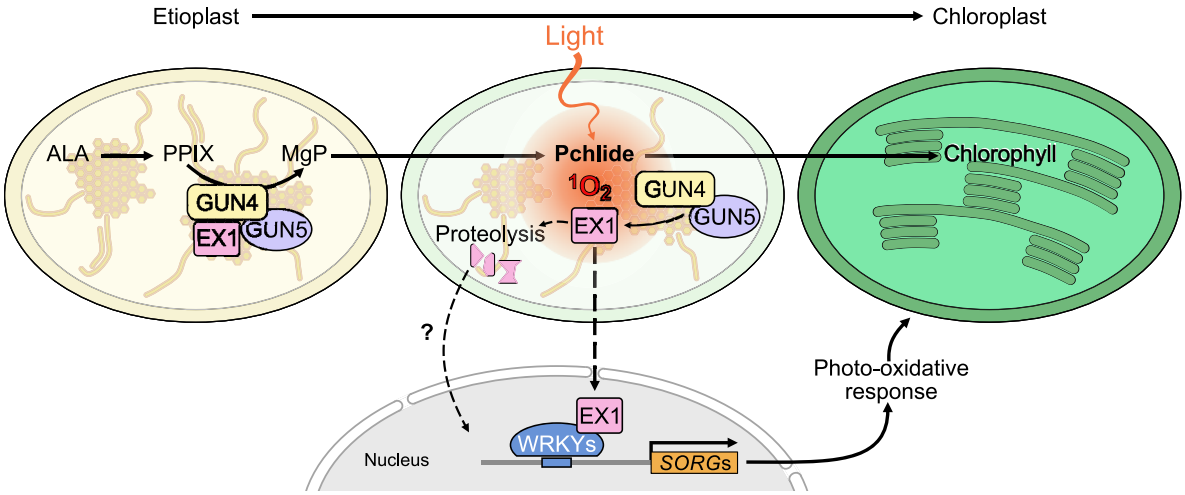

Figure 9 A working model depicting the EX1-mediated $^1O_2$ signaling pathway. In the dark (no $^1O_2$), relatively low amounts of GUN4 and GUN5 interact with EX1 in plastids (etioplasts). Light exposure induces $^1O_2$ formation by tetrapyrrole intermediates (e.g. Pchlide) that releases EX1 from the GUN4/5-EX1 complex and triggers its translocation to the nucleus, where EX1 physically interacts with WRKY transcription factors (such as WRKY18 and WRKY40) to regulate SORGs expression and ultimately photo-oxidative responses. FtsH2-mediated EX1 proteolysis is also important for propagating the singlet oxygen signal as previously proposed (Dogra et al., 2019). ALA, 5-aminolevulinic acid; PPIX, protoporphyrin IX; MgP, Mg-protoporphyrin IX. How EX1 transports from the plastid to the nucleus remains unknown.

W-box (Figure 8, D and E), suggesting that WRKY18 directly binds to *SORG* chromatin. Remarkably, EX1 fused to the GAL4 DNA-binding domain (BD-EX1) significantly activated a *GAL4pro:LUC* reporter when transfected into Arabidopsis protoplasts, relative to BD alone (Figure 8F). BD-EX1N also strongly activated *LUC* expression, even with the addition of the repressor domain from ETHYLENE-RESPONSIVE FACTOR 3 (Figure 8G). These results indicate that EX1 has intrinsic transcriptional activation activity. Hence, EX1 interacts with WRKY transcription factors and activates the expression of *SORG*s in the nucleus in response to the $^1O_2$ signal.

Discussion

Our study establishes a $^1O_2$-triggered plastid retrograde signaling pathway consisting of the GUN4/GUN5-EX1-WRKYs module that bridges the long-standing communication gap between the plastids and the nucleus (Chi et al., 2013; Brzezowski et al., 2015; Chan et al., 2016; Dogra et al., 2018). We propose a working model whereby, in the absence of $^1O_2$ (darkness), GUN4 and GUN5 interact with EX1 and EX2; however, the dark-accumulated free Pchlide (photosensitizer) induces a burst of $^1O_2$ following light irradiation, which alleviates the GUN-EX1 association. EX1 is then released from the plastids by an unknown mechanism and relocates to the nucleus, where it physically interacts with WRKY transcription factors (such as WRKY18 and WRKY40) and activates *SORG*s expression, resulting in photo-oxidative responses (Figure 9). We observed an interaction between GUN4 and EX1/2 homologs from various species from the green lineage, including *Chlamydomonas reinhardtii*, *Physcomitrium patens*, and rice, suggesting that this singlet oxygen signaling cascade may be evolutionarily conserved across the plant kingdom (Supplemental Figure S15; Supplemental Table S1). This work provides not only clues as to the signals that facilitate communication between the nucleus and other organelles but also a model that integrates pathways of anterograde light signaling and retrograde $^1O_2$ signaling in response to changing light environments.

GUN4 and GUN5 are involved in $^1O_2$ retrograde signaling

The $^1O_2$-mediated plastid-to-nucleus retrograde signaling is largely unknown. In this study, we developed a system for $^1O_2$-mediated retrograde signaling during heterotrophic-to-photoheterotrophic growth upon light and RB treatments. By using this system, we identified multiple *gun4* and *gun5* mutations as suppressors of *pif1 pif3*, suggesting an important role for GUN4 and GUN5 in regulating $^1O_2$-mediated retrograde signaling. Early genetic screens for retrograde signaling mutants identified five out of six *GUN* genes belonging to the tetrapyrrole biosynthesis pathway, highlighting the involvement of the proteins/intermediates of this pathway in retrograde signaling; however, their roles and underlying mechanisms remain mostly unknown (Susek et al., 1993; Mochizuki et al., 2001; Larkin et al., 2003; Strand et al., 2003; Pfannschmidt, 2010; Woodson et al., 2011).

As components of Mg-chelatase, GUN4 and GUN5 participate in $^1O_2$ signaling most likely through affecting the enzymatic function and tetrapyrrole biosynthesis flow and consequently $^1O_2$ production. It has been demonstrated that the accumulation of photosensitizing tetrapyrrole

intermediates, such as free Pchlide, can produce $^1O_2$ upon illumination, which acts as a retrograde signal to modulate nuclear gene expression (op den Camp et al., 2003; Wagner et al., 2004; Terry and Smith, 2013; Woodson, 2019). Etiolated *pif1 pif3* seedlings accumulated an excess amount of free Pchlide, perhaps due to increased expression levels of *GUN4* and *GUN5* as well as the other tetrapyrrole metabolism genes, thus enhancing metabolic flow (Moon et al., 2008; Stephenson et al., 2009; Zhong et al., 2009; this study). Indeed, PIF3 directly regulated *GUN5* expression (Liu et al., 2013). Genetic studies suggest that GUN4/GUN5 act downstream of PIF1/PIF3 in regulating Pchlide accumulation and $^1O_2$ production (Figure 1; Supplemental Figures 3, 4, and 7). Similarly, *gun5* was also isolated as a suppressor of the *plastid ferrochelatase 2* (its enzyme catalyzes the heme branch) mutant, which accumulated $^1O_2$ after light irradiation (Woodson et al., 2015). Mutations in *GUN4* and *GUN5* can reduce Mg-chelatase activity and in consequence result in a low supply of product and levels of downstream intermediates, such as MgP and Pchlide. While knock-out mutations of *GUN4* or *GUN5* are seedling lethal (Huang and Li, 2009; Peter and Grimm, 2009), their individual knockdown leads to reduced levels of MgP and Pchlide and decreased $^1O_2$ accumulation (Supplemental Figure S7). Similarly, a mutant in the rice *GUN4* homolog had reduced levels of Pchlide and $^1O_2$ compared to WT, especially under high-light conditions (Li et al., 2021). Consequently, the *gun4* and *gun5* knockdown mutants had higher greening percentages even under high light intensities (Figure 1). Furthermore, GUN4 may function through regulating the subcellular and intraorganellar localization of Mg-chelatase and the post-translational control of the tetrapyrrole biosynthesis pathway (Peter and Grimm, 2009; Mochizuki et al., 2010).

In addition, GUN4 and GUN5 are involved in $^1O_2$ retrograde signaling by interacting with EX1. EX1 mainly resides at the grana margin regions on the thylakoid membrane, close to the site of chlorophyll biosynthesis, where the GUN4–GUN5 complex localizes (Wang and Grimm, 2015; Wang et al., 2016), providing the spatial opportunity for EX1 to physically interact with GUN4 and GUN5. We showed that GUN4/GUN5 interacted with EX1 and that the interaction was inhibited by RB treatment or illumination (Figure 3), suggesting that GUN4/GUN5-EX1 interaction can be regulated by the $^1O_2$ signal. During this process, the $^1O_2$ signal might be sensed by the putative sensor EX1, thereby causing its post-translational modification (Wang et al., 2016; Dogra et al., 2018, 2019; Wang and Apel, 2019). In addition, GUN4 and GUN5 themselves are modified by oxidative molecules (Wittmann et al., 2021), which might also contribute to the release of the GUN4/GUN5-EX1 interaction.

$^1O_2$ signal triggers the relocation of EX1 from plastids to the nucleus

Our molecular and cellular data suggest that EX1 likely serves as a mobile macromolecule that translocates from plastids/chloroplasts to the nucleus. These evidence include: (1) immunoblot assays showing that EX1 accumulated in the nuclear fractions upon RB or light treatments; (2) real-time GFP imaging revealing that EX1-GFP signals gradually increased in the nucleus but concomitantly decreased in the plastid after light exposure; (3) CHX treatment not affecting the nuclear accumulation of EX1-GFP; (4) mutation of four lysine residues abolishing the nuclear localization and function of EX1; and (5) the possible cleavage of the transit peptide of nuclear EX1 (Figures 4–6). The advantage of, EX1 being first imported to plastids may help the protein sense the plastid-derived $^1O_2$ signal, which is then relayed to the nucleus to control gene expression through the subsequent relocation of EX1. If EX1 directly moved from the cytoplasm (the site where EX1 is initially translated) to the nucleus, plastid $^1O_2$ signal would not be carried by EX1. Therefore, EX1 may act as a "ferryboat" to transmit the plastid $^1O_2$asignal efficiently from the plastid to the nucleus, despite the associated high energy cost. EX1 might relocate to the nucleus via several routes: via an unknown protein export channel located in the chloroplast envelope; by shedding of vesicles from stromules; or through vesicle-mediated protein efflux (Krupinska et al., 2020; Mullineaux et al., 2020). How EX1 is exported from plastids and enters the nucleus remains open and will be of great interest for future studies. Several proteins have also been reported to show similar localization patterns as EX1. The single-stranded DNA-binding protein Whirly1 (WHY1) in barley (*Hordeum vulgare*) was implicated as an intracellular mobile protein (Grabowski et al., 2008; Isemer et al., 2012). HEMERA (also named pTAC12, [PLASTID TRANSCRIPTIONALLY ACTIVE 12]), NUCLEAR CONTROL OF PEP ACTIVITY, REGULATOR OF CHLOROPLAST BIOGENESIS, and PAP8 (PEP-ASSOCIATED PROTEIN 8, also named pTAC6) are also dually localized to the plastids and nucleus (Nevarez et al., 2017; Yang et al., 2019; Yoo et al., 2019; Liebers et al., 2020). Dual localization is thought to be a strategy to tighten and coordinate genome-related functions in organelles and the nucleus (Krupinska et al., 2020).

FtsH2-dependent EX1 turnover in chloroplasts is necessary for mediating retrograde $^1O_2$ signaling and the conditional *flu* mutant lacking functional FtsH2 protease impairs $^1O_2$-triggered and EX1-regulated responses (Wang et al., 2016; Dogra et al., 2017). Here we revealed that intact EX1 may directly relay the chloroplast $^1O_2$ signal to the nucleus, raising the question as to how EX1 can be both degraded in chloroplasts and translocated to the nucleus. There might be at least two possibilities that need further investigation. First, EX1 is probably not fully degraded in chloroplasts or its complete degradation may take a relatively long time (Wang et al., 2016). We observed that EX1 is transiently upregulated before its turnover begins (Figure 4; Supplemental Figure S13) and that EX1 relocation from chloroplasts to the nucleus is relatively rapid, less than 30 min as tested (Figure 5). We propose that, upon $^1O_2$ induction, EX1 transiently accumulates and a certain amount of EX1 may rapidly

translocate to the nucleus and initiate changes in *SORG*s expression, while its subsequent degradation in chloroplasts likely attenuates long-term photo-oxidative responses that otherwise limits plant growth. We are uncertain whether EX1 turnover is mediated by FtsH2 under our experimental materials and conditions. Second, FtsH2-mediated degradation and nuclear targeting of EX1 might mediate different signaling pathways under varied developmental stages or circumstances. In previous studies, EX1 stability was examined in the *flu* mutant background grown under continuous light conditions followed by dark and light treatments (Wang et al., 2016; Dogra et al., 2019). It remains unknown whether the degraded EX1 fragments might regulate the WRKY18/40-mediated signaling pathway as observed in our study. In our experiments, we used etiolated seedlings of transgenic lines in the WT background for light and RB treatments. Thus, different sources of $^1O_2$ may be produced by tetrapyrrole metabolites from grana margin or ^{3}Chl from the reaction center in grana core (Krieger-Liszkay et al., 2008) that may cause the translocation and degradation of EX1 to mediate different pathways.

EX1 and EX2 interact with each other and both have similar sequences and structural domains (Dogra et al., 2022). We revealed that both EX1 and EX2 controlled $^1O_2$ retrograde signaling (Figure 2; Supplemental Figure S9). EX1 and EX2 additively regulated Pchlide accumulation in the dark, possibly through affecting the levels and/or activity of GUN4/GUN5 since they physically interact in the plastids. In agreement with this observation, the inactivation of both *EX1* and *EX2* function abrogates the up-regulation of almost all $^1O_2$-responsive genes in the *flu* mutant background (Lee et al., 2007). EX1 and EX2 also redundantly prevent seedling greening after a far-red pretreatment (Page et al., 2017). EX1 is post-translationally oxidatively modified on tryptophan 643, which is required for $^1O_2$ perception (Dogra et al., 2019). EX2 also undergoes oxidative modification and FtsH-mediated degradation, which surprisingly counteracts EX1 turnover by reducing EX1 oxidation levels, suggesting that there is an antagonistic effect of EX1 and EX2 in response to $^1O_2$ (Dogra et al., 2022). The relationship between EX1 and EX2 is possibly more complicated than expected under different circumstances.

EX1 acts as a transcriptional coregulator to control SORGs expression with WRKY transcription factors

Our study elucidates the biochemical and molecular function of EX1 that both its full-length and N terminus possess intrinsic transcriptional activation activity and thus EX1 functions as a transcriptional co-activator that helps WRKY transcription factors control downstream gene expression (Figure 8). We showed that EX1 directly interacted with WRKY transcription factors, such as WRKY18 and WRKY40. WRKY18 and WRKY40 have been implicated in regulating the transcriptome in response to both abiotic and biotic stresses (Chen et al., 2010; Birkenbihl et al., 2017). Similarly, WRKY40 and WRKY63 control the expression of nuclear genes that respond to chloroplast and mitochondrial dysfunction (van Aken et al., 2013). EX1 may be recruited to a different set of $^1O_2$-responsive genes by forming multiple heterodimers with various WRKY proteins. These WRKYs may additively or redundantly regulate SORGs expression and $^1O_2$ responses. In agreement with this notion, increased expression of *WRKY18* or *WRKY40* confers photo-oxidative responses (Figure 7). Strikingly, the N-terminal end of EX1 contains a uvrB/C motif, which is implicated in DNA-binding and protein interaction (Skorvaga et al., 2004), although it remains to be determined whether EX1 could directly regulate downstream gene expression in the nucleus. Our genetic analysis further indicated that WRKYs act downstream of EX1 to relay the $^1O_2$ signaling (Figure 7). The transcription of many *WRKY* genes is also under the regulation of $^1O_2$-triggered signaling (Gadjev et al., 2006). In addition, EX1 might modulate the $^1O_2$ signaling pathway by interacting with other transcription factors involved in ROS responses (Gadjev et al., 2006; Chen et al., 2013; Vogel et al., 2014). Our study also suggested that, in addition to their previously known role in regulating *PhANG*s expression (Susek et al., 1993), GUN4 and GUN5 are also involved in mediating the expression of *SORG*s, which further indicate that both proteins might integrate the biogenic and operational retrograde networks.

In summary, since $^1O_2$ accumulates at relatively low levels and has a short lifespan in WT seedlings during the transition from heterotrophic-to-autotrophic growth under normal light conditions, $^1O_2$ sensing by EX1 may offer the advantage of amplifying the primary $^1O_2$ signal and generating a more stable molecular message in the chloroplasts. EX1 likely serves as a molecule that transports the signal from the chloroplasts to induce nuclear SORGs expression, thereby providing a direct link to the $^1O_2$-triggered signaling pathway.

Materials and methods

Plant materials

All mutants and transgenic plants were in the Arabidopsis (*Arabidopsis thaliana*) Columbia (Col-0) accession. The *pif1 pif3* (Chen et al., 2013), *flu* (Li et al., 2019), and *wrky18 wrky40* (Birkenbihl et al., 2017) mutants and the transgenic lines *ex1 proEX1:gEX1-GFP* (Wang et al., 2016), *WRKY18-HA*, and *WRKY40-HA* (Birkenbihl et al., 2017) were described previously. The T-DNA insertion mutants *ex1-2* (SALK_002088), *ex1-3* (SALK_022735C, shown as *ex1* in all experiments), *ex2-2* (SALK_021694C), *gun4-2* (SALK_011461, Peter and Grimm, 2009), and *gun5-10* (SAIL_138_B09) were obtained from the Arabidopsis Biological Resource Center. The double, triple, and higher-order mutants were generated by genetic crossing and genotyping of the progeny. Homozygous lines were used throughout the study.

Plant growth conditions

Seeds were surface-sterilized and sown on Murashige and Skoog (MS) medium supplemented with 1% (w/v) sucrose

and 0.8% (w/v) agar. Seeds were stratified at 4°C for 3 days in the dark, then transferred to white light (~80 μmol·m^{-2}·s^{-1}) for 10 h to promote germination before transfer to a controlled growth chamber set at 22 ± 2°C under a long-day photoperiod (LD, 16-h light/8-h dark) or in the dark. Seedlings were transferred to soil when needed and allowed to grow and set seeds in LD conditions with 75% humidity. *N. benthamiana* plants were grown individually in a tray in the same growth conditions as Arabidopsis.

Bacterial and yeast growth

Escherichia coli strain DH5 or BL21 (DE3) harboring the corresponding plasmids were grown in LB medium containing 50 μg mL^{-1} ampicillin at 37°C overnight. Agrobacterium (*Agrobacterium tumefaciens*) strain GV3101 harboring the corresponding vectors were cultured in liquid LB with the appropriate antibiotics at 28°C under constant shaking overnight. Yeast (*Saccharomyces cerevisiae*) strain EGY48 or Y2H-Gold cells were cultured in YPD medium at 28°C. The yeast cells harboring the plasmids were selected and grown on synthetic defined (SD) dropout medium lacking the appropriate nutrients at 28°C.

Generation of transgenic plants

Binary constructs were introduced into Agrobacterium strain GV3101 by electroporation and the resulting positive Agrobacterium colonies were used to transform Arabidopsis WT Col-0 or *ex1-2* plants via the floral dip method (Clough and Bent, 1998). Transgenic plants were selected on MS plates containing 50 μg mL^{-1} kanamycin or 20 μg mL^{-1} Basta. Homozygous lines were confirmed based on the segregation of antibiotic resistance and PCR genotyping. At least two representative transgenic lines were used for all experiments.

Determination of percentage greening

Seedlings were grown in the dark for 5–8 days before transfer to the growth chamber in constant light and under a normal (~80 μmol·m^{-2}·s^{-1}) or high fluence rate (~300 μmol·m^{-2}·s^{-1}) for 2 days. When appropriate, different concentrations of vitamin B6 (25–100 μM) were added to the MS medium. The percentage greening was determined by scoring the number of seedlings that had developed two green cotyledons from approximately 50 seedlings for each genotype. The percentage greening of mutants/transgenic lines was always compared to that of WT from the same batch of experiment. Three independent experiments were performed. Images from representative seedlings were taken on an agar plate using a digital camera (Olympus).

Mutagenesis, genetic screening, and mapping of suppressors

EMS mutagenesis of *pif1 pif3* mutant seeds (~25,000) was performed according to a previously published method (Kim et al., 2006). M_1 seeds were sown evenly on soil (divided into 80 trays) and allowed to grow in LD conditions as described above. M_2 seeds were harvested and bulked into 320 pools. Approximately 100 M¥ seeds per pool were surface-sterilized before being plated on MS medium, allowed to germinate, grown in the dark for 6 days, and screened for the suppressor mutant phenotype after growth in white light (~80 μmol·m^{-2}·s^{-1}) for 2 days. Seedlings with a fully or partially restored greening phenotype were selected as putative *spo* mutants and transferred to soil to recover and set M_3 seeds. Most seedlings failed to turn green, as would be expected for the *pif1 pif3* double mutant. After phenotypic verification, the M_3 plants were backcrossed to the *pif1 pif3* double mutant to yield a segregating F_2 population after selfing of the F_1 progeny. The genetic segregation of the seedling greening phenotype was determined for all candidate *spo* mutants, to select suppressors caused by a single recessive mutation. F_2 plants with a normal greening ability were grown on soil and their homozygous nature was confirmed based on the lack of segregation in the F_3 generation. Genomic DNA was isolated from the leaves of BC_1F_2 plants and the concentration of the extracted DNA was determined before pooling DNA from 24–30 plants evenly for MutMap mapping as described (Abe et al., 2012).

The pooled DNAs were subjected to Illumina whole-genome sequencing with over 20× coverage. Mutations and polymorphisms (relative to the *pif1 pif3* parent) not related to the phenotype should segregate in a 1:1 ratio. Mutations and polymorphisms linked to the phenotype should show an increased proportion of the nonreference allele. Initially, mutations in *spo1-1* (G113R), *spo1-2* (P170L), *spo1-4* (G248R), *spo1-5* (P279L), *spo1-7* (M295T), *spo1-9* (P440L), *spo1-11* (G594R), and *spo1-14* (P969S) were mapped to the *GUN5* locus and *spo2-4* (S121F) and *spo2-5* (L175F) were mapped to *GUN4* locus (Figure 1A). The DNA fragments covering *GUN5* or *GUN4* were then amplified from the other *spo1* and *spo2* alleles by PCR, and point mutations were identified by sequencing. The PCR primers for fine-mapping are listed in Supplemental Data Set S1.

RB treatment

Arabidopsis seedlings were grown for 6 days in LD before transfer to liquid MS medium containing 100 μM RB and incubation in white light (~80 μmol·m^{-2}·s^{-1}) for different periods as indicated. For protoplast experiments, RB was added to the protoplast solution to a final concentration of 50 μM and incubated in white light (~40 μmol·m^{-2}·s^{-1}) for different periods as indicated in the text.

Determination of Pchlide and chlorophyll levels

Seedlings were grown in the dark for different periods as indicated in the text, homogenized in 500 μL ice-cold 80% (v/v) acetone, and incubated in the dark overnight at 4°C. After centrifugation at 13,523 rcf at 4°C for 5 min, 77K fluorescence of the samples was determined by excitation at 440 nm and scanning from 600 to 750 nm in a fluorescence spectrophotometer (Hitachi). Emission of Pchlide and chlorophyllide peaks at 636 and 675 nm, respectively. For chlorophyll measurements,

seedlings were grown in the dark for 6.5 days and exposed to light (~80 μmol·m^{-2}·s^{-1}) for 2 days. Fifty seedlings were collected, homogenized in 1 mL ice-cold 80% (v/v) acetone, and incubated in the dark overnight at 4°C. After centrifugation at 13,523 rcf at 4°C for 5 min, absorption at 665 nm (OD665) and 649 nm (OD649) was determined in a spectrophotometer. Chlorophyll contents were calculated using formulas chlorophyll a (Chl a) = 13.95 × OD665 − 6.88 ×OD649 and Chl b = 24.96 × OD649−7.32 × OD665.

Determination of MgP levels

HPLC analysis was performed as previously described (Wang et al., 2020). Seedlings were grown under long-day conditions for 3 weeks and 100 mg leaves were collected and ground to powder. Samples were mixed with 1 mL ice-cold extraction buffer (acetone: 0.1 M NH_4OH [9:1; v/v]) and then centrifuged at 16,000 g, 4°C for 20 min. Supernatants were filtered through a 0.22-μm filter and pigments were analyzed by a Waters 2545Q system equipped with fluorescence detectors and a diode array. MgP levels were quantified with the authentic standards.

Determination of SOSG fluorescence

Etiolated seedlings were exposed to white light (~80 μmol·m^{-2}·s^{-1}) for 1 h before immersion in a 10-mM SOSG (Invitrogen) solution for 2 h in the dark. The seedlings were then exposed to white light (80–300 μmol·m^{-2}·s^{-1}) for another 0.5–1 h before visualization of SOSG fluorescence with excitation at 488 nm and emission at 532 nm. Images were captured on a Zeiss LSM 980 with an Elyra7 confocal microscope and fluorescence intensity was quantified with the measure tool of Zeiss LSM 980 after background subtraction. To measure SOSG fluorescence in cotyledons and hypocotyls, at least 100 sampling dots (diameter = 100 μm, 10~15 dots in each cotyledon or hypocotyl) were collected from at least 10 seedings for each genotype. To measure SOSG fluorescence in chloroplasts and cytoplasm, signals from at least 100 sampling dots (diameter = 100 μm) in chloroplasts or cytoplasm from at least 50 cells were collected for each genotype. Regions of high autofluorescence were avoided. The parameters were set consistently.

Trypan blue staining

Six-day-old etiolated seedlings were exposed to white light (~80 μmol·m^{-2}·s^{-1}) for 1 day. The seedlings were stained with a lactophenol trypan blue solution (1.8 mL phenol, 2 mL lactic acid, 2 mL glycerol, and 2 mL of 1 mg mL^{-1} trypan blue stock solution) preheated to 65°C and vacuum-infiltrated three times for 5 min each. The samples were boiled for 3 min and rinsed gently with chloral hydrate for 4–8 h. Representative seedlings were mounted on slides and photographed on a dissecting microscope.

RT–qPCR analysis

Total RNA was extracted using an RNA Pure Plant Kit (Tiangen) and quantified spectrophotometrically at 260 nm using a Nanodrop 2000 (Thermo Fisher Scientific). Total RNA (1 μg) was treated with RNase-free DNase I (Thermo Fisher Scientific) and then subjected to first-strand cDNA synthesis using reverse transcriptase MLV (Invitrogen). Quantitative PCR was performed using a TB Green Premix ExTaq Kit (Takara) in a Light Cycler 480 instrument (Roche) according to the manufacturers' instructions. Relative transcript levels were calculated using the comparative delta-Ct method with normalization to *ACTIN2* transcript levels. Expression analysis was performed with three independent samples; primer sequences are shown in Supplemental Data Set S1.

Plasmid construction

The full-length open reading frames or fragments of *EX1*, *EX2*, *GUN5*, *GUN4*, and *WRKY15/18/40/60/70* were amplified by PCR from Col-0 cDNA. The full-length coding sequences or fragments of *GUN4* and *EX1* homologs from *Chlamydomonas renhardtii*, *Physcomitrium patens*, and rice (*Oryza sativa*) were also amplified from their corresponding cDNAs. The EX1 N termini of these homologs were determined using the MAFFT program (Katoh et al., 2017) based on the position of the EX1 N terminus in Arabidopsis. Appropriate restriction sites were included within the primers for follow-up cloning after subcloning the DNA fragments into the pEASY-Blunt Simple vector (TransGen). All clones were validated by sequencing. The following vectors were used: pGBK-T7 (Clontech), pGAD-T7 (Clontech), pB42AD (Clontech), pLacZi2μ (Lin et al., 2007), p1302-nYFP/cYFP (Walter et al., 2004), p1300-nLUC/cLUC (Chen et al., 2008), pUC-3HA (Chen et al., 2013), pSAT-EGFP-N1 (Tzfira et al., 2005), pMAL-c5X (NEB), pGEX-5X-1 (GE Healthcare), pSAT-GAL4BD, pGAL4DB-ERF3RD (Jing et al., 2013), and pCAMBIAKaBar-cFlag (Lin et al., 2016). The vectors of pRI-GFP, pRI-3FLAG, and pRI-mCherry were modified from pRI101-AN (Takara).

Specifically, for the construction of *35S:TP-GFP-EX1* and *35S:TP-EX1C-GFP*, the 46-aa EX1 chloroplast transit peptide sequence was cloned and introduced in-frame into the plasmids. When generating the *35S:TP-GFP-EX1* construct, a fragment of *EX1* lacking the transit peptide sequence was amplified, as the transit peptide sequence was already provided by the vector at the 5′ end of *GFP*. Primers for all constructs generated in this study are listed in Supplemental Data Set S2.

Yeast assays

Experiments for yeast one-hybrid (Y1H) and two-hybrid (Y2H) assays were performed following the Yeast Protocols Handbook (Clontech). For Y1H assays, the corresponding B42AD activation domain fusion constructs and various LacZ reporter plasmids (pLacZi2μ) were co-transformed into yeast strain EGY48. Positive colonies were selected on SD medium lacking Trp and Ura (−Trp−Ura) and transferred to SD medium −Trp−Ura containing 1×BU salts, 2% (w/v) galactose, 1% (w/v) raffinose and 0.1 mg mL^{-1} X-gal

(5-bromo-4-chloro-3-indolyl-β-D-galactopyranoside) for color development. Blue colonies indicate positive protein-DNA interaction. For Y2H assays, the respective combinations of GAD-fusion and GBD-fusion plasmids were co-transformed into yeast strain Y2H-Gold (Clontech) and colonies were selected on SD medium −Leu−Trp. To assess protein interaction, the transformed colonies were suspended in liquid SD medium −Leu−Trp to an OD_{600} value of 1.0. Four microliters of yeast cell suspension was spotted onto SD medium −Leu−Trp or SD medium −Leu−Trp−His−Ade and incubated at 30°C for 2–3 days. Growth on SD medium−Trp−Leu−His−Ade indicates positive protein−protein interaction.

Luciferase Complementation Imaging (LCI) assay

Agrobacterium-mediated transient LCI assays were carried out as previously described, with modifications (Walter et al., 2004). LB medium was inoculated with Agrobacterium strain GV3101 harboring the appropriate construct and incubated overnight at 28°C. The p19 plasmid of tomato bushy stunt virus was used to inhibit gene silencing. The bacterial cultures were collected by centrifugation and resuspended in infiltration buffer (10 mM MES, pH 5.7, 10 mM $MgCl_2$) to a final cell density of $OD_{600} = 1.5$, or $OD_{600} = 1.0$ for bacteria harboring p19. The appropriate bacterial suspensions were mixed in equal volumes and 200 μM acetosyringone was added before incubation at 28°C for 3–5 h. The Agrobacterium suspensions were co-infiltrated into fully expanded young leaves of 4-week-old *N. benthamiana* with a syringe. The plants were grown under LD conditions at 22°C for 2 days before luciferase signals were analyzed on a Night SHADE LB985 (Berthold Technologies) according to the manufacturer's instructions.

Transient LUC expression assay

To analyze the transcriptional activation activity of EX1, the *GAL4pro:LUC* reporter, BD-fusion effectors (BD-EX1, BD-EX1N, and BD-EX1N-ERF3), and *35S:GUS* internal control were co-transfected into Arabidopsis protoplasts using polyethylene glycol (PEG)-mediated transient transfection as previously described (Yoo et al., 2007). The transfected protoplasts were incubated in the dark for 16 h, collected by centrifugation, and incubated in 100 μL 1× cell culture lysis reagent (Promega). Five microliters of the homogenate was mixed with 15 μL of luciferase (LUC) Assay Substrate and luminescent signals were monitored using a GloMax 20/20 Luminometer equipped with a luminescence kit (Promega). To determine the internal GUS activity, 5 μL of the cell homogenate was mixed with 45 μL GUS assay buffer (1 mM 4-methylumbelliferyl β-D-glucuronide, 50 mM sodium phosphate pH 7.0, 10 mM β-mercaptoethanol, 10 mM EDTA, 0.1% [w/v] SDS and 0.1% [v/v] Triton X-100). The samples were incubated at 37°C for 30 min before terminating the reaction by the addition of 950 μL 0.2 M Na_2CO_3. GUS activity was measured with a luminometer equipped with an ultraviolet fluorescence optical kit (Promega). The relative LUC reporter level was expressed as LUC/GUS ratio.

BiFC assay

Agrobacterium colonies carrying the nYFP- and cYFP-fusion constructs were infiltrated into *N. benthamiana* leaves using the method described above. YFP fluorescence was captured using a confocal microscope (Leica TCS SP5) with excitation at 514 nm and emission collected at 520–550 nm.

GFP fluorescence imaging

For transient GFP localization assays, the constructs were introduced into *N. benthamiana* leaves via Agrobacterium-mediated infiltration. The plants were then allowed to recover for the transgenes to express under LD conditions at 22°C for 2 days. Leaf discs were mounted on a slide and fluorescence captured with a Zeiss LSM 980 with Elyra7 confocal microscope (settings: GFP, excitation 489 nm, emission 500–550 nm; mCherry, excitation 580 nm, emission 600–610 nm). Histone H3 fused to mCherry was used as a nuclear marker. For stable Arabidopsis transgenic lines, seedlings were treated with 100 μM RB or 150 μM cycloheximide (CHX) before mounting on a slide. Fluorescence was captured by confocal microscopy (Zeiss LSM 980 with Elyra7) with the same settings as above for GFP. As a nucleus marker, DAPI (4′, 6-diamidino-2-phenylindole) fluorescence was detected with excitation at 405 nm and emission at 410–490 nm.

Production of recombinant proteins

The constructs were introduced into *E. coli* (BL21 strain) and recombinant protein was induced by the addition of 0.5 mM isopropyl β-D-1-thiogalactopyranoside at 37°C for 4 h. The pelleted bacterial cells were lysed by sonication in lysis buffer (20 mM Tris−HCl pH 7.5, 150 mM NaCl). The supernatants were then incubated with nickel-nitrilotriacetic acid agarose (QIAGEN, for His fusion proteins), Glutathione Sepharose 4B (GE Healthcare, for GST fusion proteins), or Dextrin Sepharose (GE Healthcare, for MBP fusion proteins) according to manufacturer's instructions. The beads were washed in wash buffer (20 mM Tris−HCl pH 7.5, 150 mM NaCl) and the recombinant proteins were eluted with elution buffer (20 mM Tris−HCl pH 7.5, 150 mM NaCl, and 100∼200 mM imidazole [for His-tagged proteins], 10∼100 mM reduced glutathione [for GST-tagged proteins], or 10∼100 mM maltose [for MBP-tagged proteins]).

Generation of antibodies

Rabbits were immunized with recombinant protein fragments corresponding to aa 47-278 of EX1 and aa 70-265 of GUN4 to generate EX1 and GUN4 polyclonal antibodies, respectively, at PhytoAB (Beijing). The EX1 and GUN4 immune sera were purified against GST-EX1N or His-GUN4 recombinant proteins, respectively, by affinity filtration chromatography.

Total plant protein extraction and immunoblot analysis

Arabidopsis seedlings were ground into a fine powder in liquid nitrogen and homogenized in phosphate-buffered

saline (PBS) buffer containing 20 mM sodium phosphate, 150 mM NaCl, pH 7.4, 1% (v/v) Triton X-100, and 1× complete protease inhibitor cocktail (Roche) on ice for 15 min. The samples were centrifuged at 13,523 rcf at 4°C for 15 min. The supernatants were mixed with 10× loading buffer (125 mM Tris–HCl pH 6.8, 12% [w/v] SDS, 10% [v/v] glycerol, 22% [v/v] β-mercaptoethanol, 0.001% [w/v] bromophenol blue), boiled at 95°C for 10 min, and centrifuged at 13,523 rcf for 5 min at room temperature. After SDS-PAGE separation, the proteins were transferred onto a polyvinylidene fluoride membrane using a trans-blot turbo transfer system (Bio-Tad Laboratories). Immunoblotting was performed with anti-GFP (N21021, TransGen, 1:1000), anti-FLAG (F3165, Sigma, 1:1000), anti-HA (M180-3, MBL, 1:10000), anti-EX1 (1:300), anti-GUN4 (1:1000), anti-ACT (CW0264M, CWBIO, 1:10000), anti-Tic110 (AS08293, Agrisera, 1:1000), anti-Cpn60 (AS122613, Agrisera, 1:1000), anti-D1 (PHY0057, PhytoAB, 1:1000), anti-LhcB3 (AS01002, Agrisera, 1:1000), anti-Cf1β (AS05085, Agrisera, 1:1000), and anti-RbcL (AS03037A, Agrisera, 1:1000) primary antibodies. HRP-conjugated goat anti-rabbit (CW0103, CWBIO, 1:10000) or HRP-conjugated goat anti-mouse (CW0102, CWBIO, 1:10000) antibodies were used as the secondary antibodies. The blotting signals were captured with a Chemiluminescence Imaging System (Biostep) according to the manufacturer's instructions.

Isolation of nuclear proteins

Seedlings were grown under the conditions specified in the text. One gram of Arabidopsis seedlings was ground into a fine powder in liquid nitrogen and divided equally into four 1.5-mL tubes. The powder in each tube was resuspended in 1 mL of 4°C precooled lysis buffer (20 mM Tris–HCl, pH 7.4, 25% [v/v] glycerol, 20 mM KCl, 2 mM EDTA, 2.5 mM $MgCl_2$, 250 mM sucrose, 5 mM DTT, and 1× protease inhibitor cocktail). The samples were incubated on ice for 15 min to ensure complete lysis of the cells, followed by filtration through one layer of Miracloth (Merck Millipore) twice. After centrifugation at 1,902 rcf at 4°C for 10 min, the pellets were washed five times with 1 mL of precooled nuclear resuspension buffer I (20 mM Tris–HCl, pH 7.4, 25% [v/v] glycerol, 2.5 mM $MgCl_2$, and 0.2% [v/v] Triton X-100), followed by centrifugation at 1,902 rcf at 4°C for 3 min. The pellets from the four tubes were combined and resuspended in 600 µL of precooled buffer II (250 mM sucrose, 10 mM Tris–HCl, pH 7.5, 10 mM $MgCl_2$, 1% [v/v] Triton X-100, and 1× protease inhibitor cocktail). The resuspended pellet was carefully overlaid on top of 600 µL pre-cooled buffer III (1.7 M sucrose, 10 mM Tris–HCl, pH 7.5, 2 mM $MgCl_2$, 0.15% [v/v] Triton X-100, and 1× protease inhibitor cocktail) before centrifugation at 13,523 rcf for 45 min at 4°C. The final nuclear pellets were resuspended in 100 µL nuclei lysis buffer (50 mM Tris–HCl, pH 8.0, 10 mM EDTA, 1% [w/v] SDS) and incubated on ice for 15 min to ensure complete lysis of the nuclei. The nuclear protein samples were mixed with 10 µL 10× loading buffer, boiled at 95°C for 10 min, centrifuged for 5 min at 15,871 rcf at room temperature, separated by SDS-PAGE, followed by immunoblot analysis. Anti-RbcL antibody was used as the chloroplast marker, and anti-Histone H3 (07690, Millipore) antibody was used as the nuclear marker.

Co-immunoprecipitation (Co-IP) assay

Arabidopsis protoplasts were co-transfected with combinatorial sets of plasmids. Transfected protoplasts were treated with white light as indicated in the text or RB (50 µM) and incubated for different periods before sampling. The protoplasts were collected by centrifugation and resuspended in 1 mL Co-IP buffer (25 mM Tris–HCl, pH 7.5, 150 mM NaCl, 1 mM EDTA, 1% [v/v] Triton X-100, and 1× complete protease inhibitor cocktail). After incubation in the dark on ice for 10–15 min, the samples were centrifuged at 13,523 rcf at 4°C for 10 min. A 100-µL aliquot of the supernatants was collected for input controls and 20 µL of anti-GFP–agarose beads (LABLEAD, Beijing) added to the remaining supernatant, which was incubated for 45–60 min with gentle shaking at 4°C in the dark. The beads were collected and washed four times with wash buffer (25 mM Tris–HCl, pH 7.5, 150 mM NaCl, 1 mM EDTA, 0.5% [v/v] Triton X-100). Immunoprecipitates were analyzed by SDS-PAGE separation followed by immunoblotting with anti-HA (M180-3, MBL) and anti-GFP antibodies.

For the interaction between GUN4 and EX1, total proteins were extracted from 7-day-old Col-0, *35S:EX1-GFP*, or *ex1 proEX1:gEX1-GFP* transgenic seedlings in Co-IP buffer (10 mM Tris–HCl, pH 7.5, 100 mM NaCl, 10 mM $MgCl_2$, 1 mM EDTA, 5% [v/v] glycerol, 0.4% [v/v] NP-40, 1% [v/v] Triton X-100, 1× complete protease inhibitor cocktail, and 50 µM MG132). Proteins were immunoprecipitated with 20 µL anti-GFP–agarose beads by gentle shaking for 1 h at 4°C in the dark. The pellets were washed with wash buffer four times before subjecting the immunoprecipitates to SDS-PAGE separation followed by immunoblotting with anti-GFP and anti-GUN4 antibodies.

For the interaction between EX1 and WRKY18, total proteins were extracted from Col-0 and *WRKY18-HA* transgenic seedlings in Co-IP buffer (10 mM Tris–HCl, pH 7.5, 100 mM NaCl, 10 mM $MgCl_2$, 1 mM EDTA, 5% [v/v] glycerol, 0.4% [v/v] NP-40, 1× complete protease inhibitor cocktail, and 50 µM MG132). Proteins were incubated with 1 µL of anti-HA antibody at 4°C for 1 h, followed by incubation with 20 µL protein G beads for another 2 h. The pellets were washed in wash buffer (10 mM Tris–HCl, pH 7.5, 50 mM NaCl, 10 mM $MgCl_2$, 1 mM EDTA, 5% [v/v] glycerol, 0.2% [v/v] NP-40) four times. Protein samples were separated by SDS-PAGE followed by transfer to membrane for immunoblotting with anti-HA and anti-EX1 antibodies.

Chromatin Immunoprecipitation (ChIP) assay

WRKY18-HA seedlings were grown in the dark for 6.5 days and transferred to high light (200 $\mu mol \cdot m^{-2} \cdot s^{-1}$) for 1 h. Seedlings (1 g) were crosslinked for 10 min in extraction

buffer 1 (400 mM sucrose, 10 mM Tris–HCl, pH 8.0, 5 mM β-mercaptoethanol) with 1% (v/v) formaldehyde under vacuum. Crosslinking was stopped by adding glycine to a final concentration of 125 mM. The crosslinked seedlings were ground into a fine powder in liquid nitrogen and resuspended in 30 mL of pre-cooled extraction buffer 1 with 0.1 mM PMSF and 1× protease inhibitor cocktail (Roche). The samples were filtered through Miracloth (Merck Millipore) and centrifuged at 2,880 ×*g* 4°C for 20 min. The nuclear pellets were resuspended and washed twice with 1 mL of pre-cooled extraction buffer 2 (250 mM sucrose, 10 mM Tris–HCl, pH 8.0, 10 mM $MgCl_2$, 1% [v/v] Triton X-100, 5 mM β-mercaptoethanol, 0.1 mM PMSF and 1× protease inhibitor cocktail) followed by centrifugation at 12,000 ×*g* at 4°C for 10 min. The pellets were resuspended in 300 µL of pre-cooled extraction buffer 3 (1.7 M sucrose, 10 mM Tris–HCl, pH 8.0, 2 mM $MgCl_2$, 0.15% [v/v] Triton X-100, 5 mM β-mercaptoethanol, 0.1 mM PMSF and 1× protease inhibitor cocktail). These resuspensions were carefully overlaid on top of 300 µL pre-cooled extraction buffer 3. The samples were centrifuged at 16,000 ×*g* 4°C for 1 h. The final nuclear pellets were resuspended in 300 µL nuclei lysis buffer (50 mM Tris–HCl, pH 8.0, 10 mM EDTA, 1% [w/v] SDS, 0.1 mM PMSF, and 1× protease inhibitor cocktail). The chromatin complexes were sonicated to shear DNAs into 0.5 to 2 kb fragments before centrifugation at 16,000 ×*g* 4°C for 5 min. Input DNA was aliquoted at this stage. The sonicated chromatin complex was then diluted ten times using dilution buffer (1.1% [v/v] Triton X-100, 1.2 mM EDTA, 16.7 mM Tris–HCl, pH 8.0, 167 mM NaCl, 0.1 mM PMSF and 1× protease inhibitor cocktail) and immunoprecipitated using anti-HA antibodies at 4°C with gentle agitation overnight. The samples were incubated with protein G agarose (Roche) for 3 h at 4°C with gentle agitation. The immunoprecipitated samples were washed with pre-cooled low salt wash buffer (150 mM NaCl, 0.1% [v/v] SDS, 1% [v/v] Triton X-100, 2 mM EDTA, and 20 mM Tris–HCl, pH 8.0), high salt wash buffer (500 mM NaCl, 0.1% [v/v] SDS, 1% [v/v] Triton X-100, 2 mM EDTA, and 20 mM Tris–HCl, pH 8.0), LiCl wash buffer (250 mM LiCl, 1% [v/v] NP-40, 1% [w/v] sodium deoxycholate, 1 mM EDTA, and 10 mM Tris–HCl, pH 8.0), and TE buffer (10 mM Tris–HCl, pH 8.0, and 1 mM EDTA). The crosslinked chromatin was eluted with 125 µL of freshly prepared elution buffer (1% [w/v] SDS and 0.1M $NaHCO_3$) twice. The crosslinking of the eluates as well as the input was reversed by adding 10 µL of 5 M NaCl at 65°C overnight. After reverse crosslinking, the samples were treated with 1 µL of 20 mg mL^{-1} proteinase K (Thermo Fisher Scientific) as well as 5 µL of 0.5 M EDTA and 10 µL of 1M Tris–HCl (pH 6.5) for 1 h at 45°C. The DNA was purified using QIAquick PCR Purification Kit (QIAGEN) and analyzed by quantitative PCR. The values were normalized to the input DNA. Primers for the ChIP-qPCR are listed in Supplemental Data Set S1.

Evolutionary analysis

The Arabidopsis EX and GUN4 protein sequences were used as queries to search for related proteins in 58 plant species (Supplemental Table S1), represented in Phytozome (https://phytozome.jgi.doe.gov/), and in Norway spruce (*Picea abies*; Nystedt et al., 2013), following a previously reported method (Guo, 2013).

Statistical analysis

Two-tailed paired Student's *t* tests and two-way analysis of variance (ANOVA) were performed in Microsoft Excel. Asterisks indicate statistical significance * for $P < 0.05$ and ** for $P < 0.01$. All related analyses are shown in Supplemental Data Set S3.

Accession numbers

DNA sequences of all genes in this study were extracted from TAIR with the gene ID listed below: *PIF1* (At2g20180), *PIF3* (At1g09530), *EX1* (At4g33630), *EX2* (At1g27510), *FLU* (At3g14110), *GUN4* (At3g59400), *GUN5* (At5g13630), *ERF4* (At3g15210), *SIB1* (At3g56710), *ZAT12* (At5g59820), *WRKY33* (At2g38470), *WRKY18* (At4g31800), *WRKY40* (At1g80840), *WRKY60* (At2g25000), *WRKY15* (At2g23320), *WRKY70* (At3g56400), *NHL3* (At5g06320), and At3g2900.

Supplemental data

The following materials are available in the online version of this article.

Supplemental Figure S1. Establishment of the light-triggered seedling greening system using *pif1 pif3*.

Supplemental Figure S2. Sequence alignment of GUN4 and GUN5.

Supplemental Figure S3. Suppressor screening for *spo* mutants.

Supplemental Figure S4. Characterization of the *gun4* or *gun5* mutations and their effects on *pif1 pif3*.

Supplemental Figure S5. Genetic interaction with the *flu* mutant.

Supplemental Figure S6. PIF1 and PIF3 regulate the expression levels of *GUN4* and *GUN5*.

Supplemental Figure S7. Determination of tetrapyrrole biosynthesis intermediates and seedling greening.

Supplemental Figure S8. Etiolated seedlings overexpressing *GUN4* are sensitive to light.

Supplemental Figure S9. Analysis of Pchlide levels in dark-grown seedlings.

Supplemental Figure S10. GUN4 interacts with N-terminal EX1/EX2.

Supplemental Figure S11. Determination of the specificity of RB treatment.

Supplemental Figure S12. Characterization of *EX1* transgenic lines.

Supplemental Figure S13. Immunoblot analysis of EX1 and chloroplast-localized proteins.

Supplemental Figure S14. Interaction between EX1/EX2 and WRKY transcription factors.

Supplemental Figure S15. Evolutionary analysis of the EX-GUN4 interaction.

Supplemental Table S1. List of plant species used in the evolutionary analysis.

Supplemental Data Set S1. List of oligonucleotides used in this study.

Supplemental Data Set S2. List of primers for constructing plasmids.

Supplemental Data Set S3. Statistical analysis.

Acknowledgments

We are grateful to Dr. Chanhong Kim (Shanghai Center for Plant Stress Biology, Chinese Academy of Sciences) for providing the *ex1 proEX1:gEX1-GFP* line, Dr. Imre Somssich (Max-Planck-Institute for Plant Breeding Research) for providing *wrky18 wrky40* mutant and *WRKY18* and *WRKY40* transgenic lines, Dr. Bernhard Grimm (Humboldt-Universität zu Berlin) for providing the anti-GUN5 antibody, and the Arabidopsis Biological Resource Center for providing T-DNA insertion lines. We thank Jingquan Li for confocal microscopy technical support and Drs. Xing Wang Deng and Haiyang Wang for critical comments on the manuscript.

Funding

This work was supported by grants from the National Natural Science Foundation of China (32030009), the National Key Research and Development Program of China (2020YFA0907600, 2019YFA0904600), and the Strategic Priority Research Program of the Chinese Academy of Sciences (XDB27030205).

Conflict of interest statement. None declared.

References

Abe A, Kosugi S, Yoshida K, Natsume S, Takagi H, Kanzaki H, Matsumura H, Yoshida K, Mitsuoka C, Tamiru M, et al. (2012) Genome sequencing reveals agronomically important loci in rice using MutMap. Nat Biotechnol **30**: 174–178

Adhikari ND, Froehlich JE, Strand DD, Buck SM, Kramer DM, Larkin RM (2011) GUN4-porphyrin complexes bind the ChlH/GUN5 subunit of Mg-chelatase and promote chlorophyll biosynthesis in Arabidopsis. Plant Cell **23**: 1449–1467

Apel K, Hirt H (2004) Reactive oxygen species: metabolism, oxidative stress, and signaling transduction. Annu Rev Plant Biol **55**: 373–399

Birkenbihl RP, Kracher B, Roccaro M, Somssich IE (2017) Induced genome-wide binding of three Arabidopsis WRKY transcription factors during early MAMP-triggered immunity. Plant Cell **29**: 20–38

Brzezowski P, Richter AS, Grimm B (2015) Regulation and function of tetrapyrrole biosynthesis in plants and algae. Biochim Biophys Acta **1847**: 968–985

Chan KX, Phua SY, Crisp P, McQuinn R, Pogson BJ (2016) Learning the languages of the chloroplast: retrograde signaling and beyond. Annu Rev Plant Biol **67**: 25–53

Chen D, Xu G, Tang W, Jing Y, Ji Q, Fei Z, Lin R (2013) Antagonistic bHLH/bZIP transcription factors form transcriptional modules that integrate light and reactive oxygen species signaling in *Arabidopsis*. Plant Cell **25**: 1657–1673

Chen H, Lai Z, Shi J, Xiao Y, Chen Z, Xu X (2010) Roles of Arabidopsis WRKY18, WRKY40 and WRKY60 transcript factors in plant responses to abscisic acid and abiotic stress. BMC Plant Biol **10**: 281

Chen H, Zou Y, Shang Y, Lin H, Wang Y, Cai R, Tang X, Zhou JM (2008) Firefly luciferase complementation imaging assay for protein–protein interactions in plants. Plant Physiol **146**: 368–376

Chi W, Sun X, Zhang L (2013) Intracellular signaling from plastid to nucleus. Annu Rev Plant Biol **64**: 559–582

Clough SJ, Bent AF (1998) Floral dip: a simplified method for *Agrobacterium*-mediated transformation of *Arabidopsis thaliana*. Plant J **16**: 735–743

de Souza A, Wang JZ, Dehesh K (2017) Retrograde signals: integrators of interorganellar communication and orchestrators of plant development. Annu Rev Plant Biol **68**: 85–108

Dogra V, Duan J, Lee KP, Lv S, Liu R, Kim C (2017) FtsH2-dependent proteolysis of EXECUTER1 is essential in mediating singlet oxygen-triggered retrograde signaling in *Arabidopsis thaliana*. Frontiers Plant Sci **8**: 1145

Dogra V, Li M, Singh S, Li M, Kim C (2019) Oxidative post-translational modification of EXECUTER1 is required for singlet oxygen sensing in plastids. Nat Commun **10**: 2834

Dogra V, Rochaix JD, Kim C (2018) Singlet oxygen-triggered chloroplast-to-nucleus retrograde signalling pathways: an emerging perspective. Plant Cell Environ **41**: 1727–1738

Dogra V, Singh RM, Li M, Li M, Singh S, Kim C (2022) EXECUTER2 modulates the EXECUTER1 signalosome through its singlet oxygen-dependent oxidation. Mol Plant **15**: 438–453

Flors C, Fryer MJ, Waring J, Reeder B, Bechtold U, Mullineaux PM, Nonell S, Wilson MT, Baker NR (2006) Imaging the production of singlet oxygen in vivo using a new fluorescent sensor, singlet oxygen sensor green. J Exp Bot **57**: 1725–1734

Gadjev I, Vanderauwera S, Gechev TS, Laloi C, Minkov IN, Shulaev V, Apel K, Inzé D, Mittler R, Van Breusegem F (2006) Transcriptomic footprints disclose specificity of reactive oxygen species signaling in Arabidopsis. Plant Physiol **141**: 436–445

Grabowski E, Miao Y, Mulisch M, Krupinska K (2008) Single-strand DNA-binding protein Whirly1 in barley leaves is located in plastids and the nucleus of the same cell. Plant Physiol **147**: 1800–1804

Guo YL (2013) Gene family evolution in green plants with emphasis on the origination and evolution of *Arabidopsis thaliana* genes. Plant J **73**: 941–951

Hernández-Verdeja T, Strand Å (2018) Retrograde signals navigate the path to chloroplast development. Plant Physiol **176**: 967–976

Hernández-Verdeja T, Vuorijoki L, Strand Å (2020) Emerging from the darkness: interplay between light and plastid signaling during chloroplast biogenesis. Physiol Plant **169**: 397–406

Hohmann-Marriott MF, Blankenship RE (2011) Evolution of photosynthesis. Annu Rev Plant Biol **62**: 515–548

Huang Y-S, Li H-M (2009) Arabidopsis CHLI2 can substitute for CHLI1. Plant Physiol **150**: 636–645

Huq E, Al-Sady B, Hudson M, Kim CH, Apel K, Quail PH (2004) Phytochrome-interacting factor 1 is a critical bHLH regulator of chlorophyll biosynthesis. Science **305**: 1937–1941

Isemer R, Mulisch M, Schäfer A, Kirchner S, Koop HU, Krupinska K (2012) Recombinant Whirly1 translocates from transplastomic chloroplasts to the nucleus. FEBS Lett **586**: 85–88

Jing Y, Zhang D, Wang X, Tang W, Wang W, Huai J, Xu G, Chen D, Li Y, Lin R (2013) Arabidopsis chromatin-remodeling factor PICKLE interacts with transcription factor HY5 to regulate hypocotyl cell elongation. Plant Cell **25**: 242–256

Katoh K, Rozewicki J, Yamada KD (2017) MAFFT online service: multiple sequence alignment, interactive sequence choice and visualization. Brief Bioinform **20**: 1160–1166

Kim C, Apel K (2013) Singlet oxygen-mediated signaling in plants: moving from *flu* to wild type reveals an increasing complexity. Photosynth Res **116**: 455–464

Kim C, Lee KP, Baruah A, Nater M, Göbel C, Feussner I, Apel K (2009) $^1O_2$-mediated retrograde signaling during late embryogenesis predetermines plastid differentiation in seedlings by recruiting abscisic acid. Proc Natl Acad Sci USA **106**: 9920–9924

Kim Y, Schumaker KS, Zhu J-K (2006) EMS mutagenesis of Arabidopsis. *In* Salinas J, Sanchez-Serrano JJ, eds, From: Methods in Molecular Biology, Vol 323: Arabidopsis Protocols, Ed 2. © Humana Press Inc., Totowa, NJ, pp 101–103

Kosugi S, Hasebe M, Tomita M, Yanagawa H (2009) Systematic identification of yeast cell cycle-dependent nucleocytoplasmic shuttling proteins by prediction of composite motifs. Proc Natl Acad Sci USA **106**: 10171–10176

Koussevitzky S, Nott A, Mockler TC, Hong F, Sachetto-Martins G, Surpin M, Lim J, Mittler R, Chory J (2007) Signals from chloroplasts converge to regulate nuclear gene expression. Science **316**: 715–719

Krieger-Liszka A, Christian F, Achim T (2008) Singlet oxygen production in photosystem II and related protection mechanism. Photosyn Res **98**: 551–564

Krupinska K, Blanco NE, Oetke S, Zottini M (2020) Genome communication in plants mediated by organelle–nucleus-located proteins. Philos Trans R Soc Lond B Biol Sci **375**: 20190397

Laloi C, Stachowiak M, Pers-Kamczyc E, Warzych E, Murgia I, Apel K (2007) Cross-talk between singlet oxygen- and hydrogen peroxide-dependent signaling of stress responses in *Arabidopsis thaliana*. Proc Natl Acad Sci USA **104**: 672–677

Lamberts JJM, Neckers DC (1985) Rose Bengal derivatives as singlet oxygen sensitizers. Tetrahedron **41**: 2183–2190

Larkin RM, Alonso JM, Ecker JR, Chory J (2003) GUN4, a regulator of chlorophyll synthesis and intracellular signaling. Science **299**: 902–906

Lee KP, Kim C, Landgraf F, Apel K (2007) EXECUTER1- and EXECUTER2-dependent transfer of stress-related signals from the plastid to the nucleus of *Arabidopsis thaliana*. Proc Natl Acad Sci USA **104**: 10270–10275

Li R-Q, Jiang M, Huang J-Z, Moller IM, Shu Q-Y (2021) Mutations in the *genomes uncoupled 4* gene cause ROS accumulation and repress expression off peroxidase genes in rice. Front Plant Sci **12**: 682453

Li Z, Mo W, Jia L, Xu YC, Tang W, Yang W, Guo YL, Lin R (2019) Rice FLUORESCENT1 is involved in the regulation of chlorophyll. Plant Cell Physiol **60**: 2307–2318

Liebers M, Gillet FX, Israel A, Pounot K, Chambon L, Chieb M, Chevalier F, Ruedas R, Favier A, Gans P, et al. (2020) Nucleo-plastidic PAP8/pTAC6 couples chloroplast formation with photomorphogenesis. EMBO J **39**: e104941

Lin R, Ding L, Casola C, Ripoll DR, Feschotte C, Wang H (2007) Transposase-derived transcription factors regulate light signaling in *Arabidopsis*. Science **318**: 1302–1305

Lin XL, Niu D, Hu ZL, Kim DH, Jin YH, Cai B, Liu P, Miura K, Yun DJ, Kim WY, et al. (2016) An Arabidopsis SUMO E3 ligase, SIZ1, negatively regulates photomorphogenesis by promoting COP1 activity. PLoS Genet **12**: e1006016

Liu X, Chen CY, Wang KC, Luo M, Tai R, Yuan LY, Zhao M L, Yang SG, Tian G, Cui YH, et al. (2013) PHYTOCHROME INTERACTING FACTOR3 associates with the histone deacetylase HDA15 in repression of chlorophyll biosynthesis and photosynthesis in etiolated Arabidopsis seedlings. Plant Cell **25**: 1258–1273

Meskauskiene R, Nater M, Goslings D, Kessler F, op den Camp R, Apel K (2001) FLU: a negative regulator of chlorophyll biosynthesis in *Arabidopsis thaliana*. Proc Natl Acad Sci USA **98**: 12826–12831

Mochizuki N, Brusslan JA, Larkin R, Nagatani A, Chory J (2001) *Arabidopsis genomes uncoupled 5* (*GUN5*) mutant reveals the involvement of Mg-chelatase H subunit in plastid-to-nucleus signal transduction. Proc Natl Acad Sci USA **98**: 2053–2058

Mochizuki N, Tanaka R, Grimm B, Masuda T, Moulin M, Smith AG, Tanaka A, Terry MJ (2010) The cell biology of tetrapyrroles: a life and death struggle. Trends Plant Sci **15**: 488–498

Moon J, Zhu L, Shen H, Huq E (2008) PIF1 directly and indirectly regulates chlorophyll biosynthesis to optimize the greening process in Arabidopsis. Proc Natl Acad Sci USA **105**: 9433–9438

Mullineaux PM, Exposito-Rodriguez M, Laissue PP, Smirnoff N, Park E (2020) Spatial chloroplast-to-nucleus signalling involving plastid–nuclear complexes and stromules. Philos Trans R Soc Lond B Biol Sci **375**: 20190405

Nevarez PA, Qiu Y, Inoue H, Yoo CY, Benfey PN, Schnell DJ, Chen M (2017) Mechanism of dual targeting of the phytochrome signaling component HEMERA/pTAC12 to plastids and the nucleus. Plant Physiol **173**: 1953–1966

Ni M, Tepperman JM, Quail PH (1998) PIF3, a phytochrome-interacting factor necessary for normal photoinduced signal transduction, is a novel basic helix-loop-helix protein. Cell **95**: 657–667

Nott A, Jung HS, Koussevitzky S, Chory J (2006) Plastid-to-nucleus retrograde signaling. Annu Rev Plant Biol **57**: 739–759

Nystedt B, Street NR, Wetterbom A, Zuccolo A, Lin YC, Scofield DG, Vezzi F, Delhomme N, Giacomello S, Alexeyenko A, et al. (2013) The Norway spruce genome sequence and conifer genome evolution. Nature **497**: 579–584

op den Camp RG, Przybyla D, Ochsenbein C, Laloi C, Kim C, Danon A, Wagner D, Hideg E, Göbel C, Feussner I, et al. (2003) Rapid induction of distinct stress responses after the release of singlet oxygen in Arabidopsis. Plant Cell **15**: 2320–2332

Page MT, McCormac AC, Smith AG, Terry MJ (2017) Singlet oxygen initiates a plastid signal controlling photosynthetic gene expression. New Phytol **213**: 1168–1180

Peter E, Grimm B (2009) GUN4 is required for posttranslational control of plant tetrapyrrole biosynthesis. Mol Plant **2**: 1198–1210

Pfannschmidt T (2010) Plastidial retrograde signalling—a true "plastid factor" or just metabolite signatures? Trends Plant Sci **15**: 427–435

Pogson BJ, Woo NS, Förster B, Small ID (2008) Plastid signaling to the nucleus and beyond. Trends Plant Sci **13**: 602–609

Ramel F, Ksas B, Akkari E, Mialoundama AS, Monnet F, Krieger-Liszkay A, Ravanat JL, Mueller MJ, Bouvier F, Havaux M (2013) Light-induced acclimation of the Arabidopsis *chlorinal* mutant to singlet oxygen. Plant Cell **25**: 1445–1462

Rushton PJ, Somssich IE, Ringler P, Shen QJ (2010) WRKY transcription factors. Trends Plant Sci **15**: 247–258

Shin J, Kim K, Kang H, Zulfugarov IS, Bae G, Lee CH, Lee D, Choi G (2009) Phytochromes promote seedling light responses by inhibiting four negatively-acting phytochrome-interacting factors. Proc Natl Acad Sci USA **106**: 7660–7665

Skorvaga M, DellaVecchia MJ, Croteau DL, Theis K, Truglio JJ, Mandavilli BS, Kisker C, Van Houten B (2004) Identification of residues within UvrB that are important for efficient DNA binding and damage processing. J Biol Chem **279**: 51574–51580

Stephenson PG, Fankhauser C, Terry MJ (2009) PIF3 is a repressor of chloroplast development. Proc Natl Acad Sci USA **106**: 7654–7659

Strand Å, Asami T, Alonso J, Ecker JR, Chory J (2003) Chloroplast to nucleus communication triggered by accumulation of Mg-protoporphyrinIX. Nature **421**: 79–83

Susek RE, Ausubel FM, Chory J (1993) Signal transduction mutants of Arabidopsis uncouple nuclear *CAB* and *RBCS* gene expression from chloroplast development. Cell **74**: 787–799

Tanaka R, Kobayashi K, Masuda T (2011) Tetrapyrrole metabolism in *Arabidopsis thaliana*. Arabidopsis Book **9**: e0145

Tarahi Tabrizi S, Sawicki A, Zhou S, Luo M, Willows RD (2016) GUN4-protoporphyrin IX is a singlet oxygen generator with consequences for plastid retrograde signaling. J Biol Chem **291**: 8978–8984

Terry MJ, Smith AG (2013) A model for tetrapyrrole synthesis as the primary mechanism for plastid-to-nucleus signaling during chloroplast biogenesis. Front Plant Sci **4**: 14

Triantaphylidès C, Havaux M (2009) Singlet oxygen in plants: production, detoxification and signaling. Trends Plant Sci **14**: 219–228

Triantaphylidès C, Krischke M, Hoeberichts FA, Ksas B, Gresser G, Havaux M, Van Breusegem F, Mueller MJ (2008) Singlet oxygen is the major reactive oxygen species involved in photooxidative damage to plants. Plant Physiol **148**: 960–968

Tzfira T, Tian GW, Lacroix B, Vyas S, Li J, Leitner-Dagan Y, Krichevsky A, Taylor T, Vainstein A, Citovsky V (2005) pSAT vectors: a modular series of plasmids for autofluorescent protein tagging and expression of multiple genes in plants. Plant Mol Biol **57**: 503–516

Van Aken O, Zhang B, Law S, Narsai R, Whelan J (2013) AtWRKY40 and AtWRKY63 modulate the expression of stress-responsive nuclear genes encoding mitochondrial and chloroplast proteins. Plant Physiol **162**: 254–271

Vogel MO, Moore M, König K, Pecher P, Alsharafa K, Lee J, Dietz KJ (2014) Fast retrograde signaling in response to high light involves metabolite export, MITOGEN-ACTIVATED PROTEIN KINASE6, and AP2/ERF transcription factors in Arabidopsis. Plant Cell **26**: 1151–1165

Wagner D, Przybyla D, Op den Camp R, Kim C, Landgraf F, Lee KP, Würsch M, Laloi C, Nater M, Hideg E, et al. (2004) The genetic basis of singlet oxygen-induced stress responses of *Arabidopsis thaliana*. Science **306**: 1183–1185

Walter M, Chaban C, Schütze K, Batistic O, Weckermann K, Näke C, Blazevic D, Grefen C, Schumacher K, Oecking C, et al. (2004) Visualization of protein interactions in living plant cells using bimolecular fluorescence complementation. Plant J **40**: 428–438

Wang L, Apel K (2019) Dose-dependent effects of $^1O_2$ in chloroplasts are determined by its timing and localization of production. J Exp Bot **70**: 29–40

Wang L, Kim C, Xu X, Piskurewicz U, Dogra V, Singh S, Mahler H, Apel K (2016) Singlet oxygen- and EXECUTER1-mediated signaling is initiated in grana margins and depends on the protease FtsH2. Proc Natl Acad Sci USA **113**:E3792–E3800

Wang P, Grimm B (2015) Organization of chlorophyll biosynthesis and insertion of chlorophyll into the chlorophyll-binding proteins in chloroplasts. Photosynth Res **126**: 189–202

Wang P, Richter AS, Kleeberg JRW, Geimer S, Grimm B (2020) Post-translational coordination of chlorophyll biosynthesis and breakdown by BCMs maintains chlorophyll homeostasis during leaf development. Nat Commun **11**: 1–17

Wittmann D, Sinha N, Grimm B (2021) Thioredoxin-dependent control balances the metabolic activities of tetrapyrrole biosynthesis. Biol Chem **402**: 379–397

Woodson JD (2019) Chloroplast stress signals: regulation of cellular degradation and chloroplast turnover. Curr Opin Plant Biol **52**: 30–37

Woodson JD, Joens MS, Sinson AB, Gilkerson J, Salomé PA, Weigel D, Fitzpatrick JA, Chory J (2015) Ubiquitin facilitates a quality-control pathway that removes damaged chloroplasts. Science **350**: 450–454

Woodson JD, Perez-Ruiz JM, Chory J (2011) Heme synthesis by plastid ferrochelatase I regulates nuclear gene expression in plants. Curr Biol **21**: 897–903

Wu GZ, Bock R (2021) GUN Control in retrograde signaling: how GENOMES UNCOUPLED proteins adjust nuclear gene expression to plastid biogenesis. Plant Cell **33**: 457–474

Wu GZ, Meyer EH, Richter AS, Schuster M, Ling Q, Schöttler MA, Walther D, Zoschke R, Grimm B, et al. (2019) Control of retrograde signalling by protein import and cytosolic folding stress. Nat Plants **5**: 525–538

Yang EJ, Yoo CY, Liu J, Wang H, Cao J, Li FW, Pryer KM, Sun TP, Weigel D, Zhou P, et al. (2019) NCP activates chloroplast transcription by controlling phytochrome-dependent dual nuclear and plastidial switches. Nat Commun **10**: 2630

Yoo SD, Cho YH, Sheen J (2007) *Arabidopsis* mesophyll protoplasts: a versatile cell system for transient gene expression analysis. Nat Protocols **2**: 1565–1572

Yoo CY, Pasoreck EK, Wang H, Cao J, Blaha GM, Weigel D, Chen M (2019) Phytochrome activates the plastid-encoded RNA polymerase for chloroplast biogenesis via nucleus-to-plastid signaling. Nat Commun **10**: 2629

Zhang S, Apel K, Kim C (2014) Singlet oxygen-mediated and EXECUTER-dependent signalling and acclimation of *Arabidopsis thaliana* exposed to light stress. Philos Trans R Soc Lond B Biol Sci **369**: 20130227

Zhong SW, Zhao MT, Shi TY, Shi H, An FY, Zhao Q, Guo HW (2009) EIN3/EIL1 cooperate with PIF1 to prevent photo-oxidation and to promote greening of Arabidopsis seedlings. Proc Natl Acad Sci USA **106**: 21431–21436